LATVIAN JOURNAL of PHYSICS and TECHNICAL SCIENCES

ISSN 0868 - 8257

1

(Vol. 60)

2023

CONTENTS

LATVIAN JOURNAL of PHYSICS and TECHNICAL SCIENCES

LATVIJAS FIZIKAS un TEHNISKO ZINĀTŅU ŽURNĀLS

ЛАТВИЙСКИЙ ФИЗИКО-ТЕХНИЧЕСКИЙ ЖУРНАЛ

Published six times a year since February 1964
Iznāk sešas reizes gadā kopš 1964. gada februāra
Выходит шесть раз в год с февраля 1964 года

1 (Vol. 60) • 2023

RĪGA

Language Editor: O. Ivanova
Computer Designer: I. Begicevs

INDEXED (PUBLISHED) IN

www.scopus.com
www.sciendo.com
EBSCO (Academic Search Complete, www.epnet.com), INSPEC (www.iee.org.com).
VINITI (www.viniti.ru), Begell House Inc/ (EDC, www.edata-center.com).

Issuers: Institute of Physical Energetics,
Institute of Solid State Physics, University of Latvia
Registration Certificate Number: 000700221

Editorial Contacts:
14 Dzerbenes Street, Riga, LV - 1006
Ph.: + 371 67551732
E-mail: leo@lza.lv
www.fei-web.lv

sciendo

LATVIAN JOURNAL OF PHYSICS
AND TECHNICAL SCIENCES
2023, N 1

DOI: 10.2478/lpts-2023-0001

INTERACTION BEHAVIORS OF LONGITUDINAL AND TRANSVERSE SEISMIC WAVES WITH UNDERGROUND GEOENGINEERING OBJECTS

N. Remez[1], A. Dychko[1*], T. Hrebeniuk[1], A. Kraychuk[2],
S. Kraychuk[2], N. Ostapchuk[2]

[1] National Technical Universty of Ukraine
"Igor Sikorsky Kyiv Polytechnic Institute"
37 Peremohy Ave., Kyiv, 03056, UKRAINE
[2] Rivne State University of Humanities
12 Stepana Bandery Str., Rivne, 33028, UKRAINE
*e-mail: aodi@ukr.net

Main pipelines as long linear objects are vulnerable to dangerous natural and man-made influences. One of the technogenic source is large-scale explosions, which cause a sharp fluctuations of soil and cause serious damage to underground pipelines. When calculating the strength of pipeline systems, it is assumed that the damage occurs mainly due to additional axial stretching. However, the destruction and damage of pipelines can occur during seismic impacts directed perpendicular to the longitudinal axis of the pipeline.

To assess the impact of longitudinal and transverse waves on the underground pipeline during seismic action a software-calculation module is developed. It implements a model of dynamic strength analysis, which allows estimating the magnitude of longitudinal and transverse seismic loads on the underground pipeline to establish safe parameters of seismic loads and geometric dimensions of the protected object. The final system of equations of motion of N nodes of a discrete system for a single length of the pipeline is presented as a system of $4N$ equations of the first order.

The efforts on the internal nodes are determined by the strain stresses at the displacement of the nodes of the adjacent rods. The efforts on the nodes of the pipe contour are the diffraction interaction of seismic waves in the soil with the pipe. The system of equations is supplemented by the corresponding initial and boundary conditions.

The dependences of the inflow of longitudinal and transverse pressure of explosive seismic pressure on the pipeline are established. The dependences of stresses in the pipeline of the diameter, thickness and type of soil are researched.

Keywords*: Combined effect of seismic load and transported product, longitudinal and transverse seismic waves, mathematical simulation, underground geoengineering objects.*

1. INTRODUCTION

Intensive development and active modernization of the system of main pipelines of the oil and gas industry are associated not only with the development of fields of new production areas and construction of pipelines, but also with the need for reliable and safe transport in difficult areas and under difficult climatic and engineering-geological conditions, and also in military territories.

Main pipelines as long linear objects are vulnerable to dangerous natural and man-made influences. One of the sources of man-made threats to pipelines is large-scale explosions, which cause sharp fluctuations in the soil and cause serious damage to underground pipelines.

When calculating the strength of pipeline systems, it is assumed that damage to the linear part of the pipeline occurs mainly due to additional axial stretching that occurs in the pipe during a seismic wave and increases when the axis of the pipeline coincides with the direction of wave propagation [1], [2]. This approach has a number of disadvantages. In particular, the effects directed normally to the longitudinal axis of the pipeline are not taken into account, as well as the design features of the linear part of the pipeline (pipe diameter, wall thickness, etc.) and, finally, the effect of pipe slippage on the ground. Interactions of seismic explosive waves with underground and surface structures are considered in [3]–[8]. It is assumed that the waves are volumetric. However, as shown in [9] and [10], the destruction and damage of pipelines can occur during seismic impacts directed perpendicular to the longitudinal axis of the pipeline.

In this regard, **the aim of the research** is to assess the impact of transverse waves on the underground pipeline during seismic action from an explosive source.

2. MATERIALS AND METHODS

Numerical modelling of the impact of longitudinal and transverse waves on the underground pipeline is carried out to predict the seismic action on the geoengineering objects.

To achieve this aim, a software-calculation module is developed, which implements the model of dynamic strength analysis [9], [11].

When studying the strength of the pipeline, taking into account the seismic impact, the following characteristics are changed: the diameter of the pipeline – 820, 1020, 1220 mm; pipe wall thickness – 12, 16, 20, 24, 28 mm; soil – sand, sandy loam (Table 1 [7]); seismic intensity of the earthquake – 7, 8, 9, 10 points. The following steel indicators are adopted: density – 7850 kg/m^3; Poisson's ratio – 0.3.

Table 1. Soil Characteristics

Type	Density, kg/m^3	The modulus of elasticity of rock, *MPa*	Specific adhesion of rock, *kPa*	Angle of internal friction, *deg*	Velocity of seismic waves in the rock, *m/s*
Granite	2300	40	2	35	150
Sandstone	1970	21	8	20	350

3. THE IMPACT OF TRANSVERSE WAVES ON THE UNDERGROUND PIPELINE

Figure 1 shows the calculation scheme of seismic action of the explosion with a non-uniform step in the spatial coordinate before and after 1 second after it. The circle indicates the position of the pipeline, the seismic wave falls to the right of the pipeline.

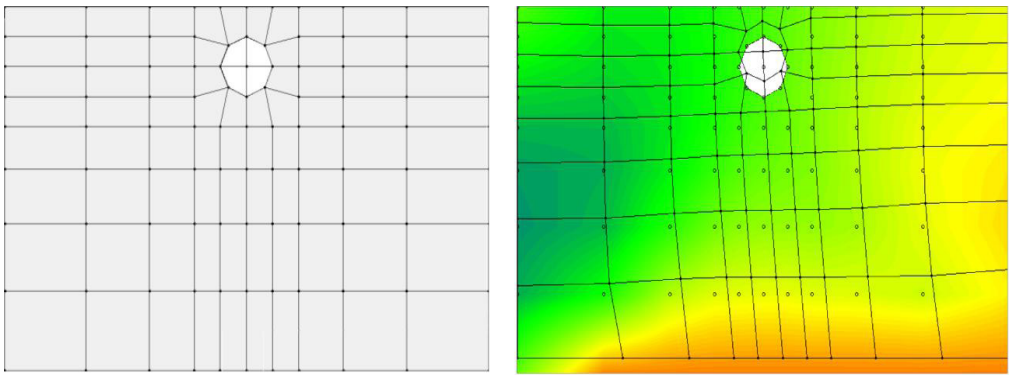

Fig. 1. Calculation scheme with a non-uniform step to the beginning (left) and during (right) seismic impact.

The final system of equations of motion of *N* nodes of a discrete system for a single length of pipeline has the form

$$\ddot{X} = P_x / m, \quad \ddot{Y} = P_y / m, \tag{1}$$

and it reduces to a system of first-order *4N* equations

$$\begin{aligned} \dot{V}_x &= P_x / m, \quad \dot{X} = V_x, \\ \dot{V}_y &= P_y / m, \quad \dot{Y} = V_y, \end{aligned} \tag{2}$$

where P_x,P_y – components of the force on the node of mass *m* in the projections on the axis of the inertial coordinate system XOY; V_x, V_y, $\dot{V}_x$, $\dot{V}_y$ – speed and acceleration of nodes.

The forces P_x, P_y on the nodes are determined by the strain stresses during shear of the nodes of the adjacent rods. The forces on the nodes of the pipe contour represent the diffraction interaction of seismic waves in the soil with the pipe.

Load from seismic impact is determined by the ratio

$$N_{xy} = \sqrt{N_x^2 + N_y^2} = P_m R, \tag{3}$$

where N_x and N_y – components of the load vector N_{xy} in the respective axes with maximum pressures: $P_x = N_x/R$ and $P_y = N_y/R$; $P_m = N_{xy}/R$ – pressures; *R* – radius of the pipe.

These seismic effects cause annular bending and compression of the wall of the shell of the pipeline. The stresses arising in the pipe have an uneven distribution and depend on the angle φ in the range of 0 ... 2π. The highest voltage values are at the points of intersection A ($\varphi = 0; \pi$) *i C* ($\varphi = \pm\pi / 2$) [11, 12]:

- normal fibre flexural stresses

$$\sigma_{MA} = \pm 0{,}305 P_m R^2 / W_k, \quad (4)$$

$$\sigma_{MC} = \pm 0{,}16847 P_m R^2 / W_k, \quad (5)$$

- normal compression stresses

$$\sigma_{NA} = -0{,}02653 P_m R / F, \quad (6)$$

$$\sigma_{NC} = -0{,}5 P_m R / F, \quad (7)$$

where $W_k = d\delta^2 / 6$ and $F = \delta d$ – moment of resistance, m^3, and the cross-sectional area of the shell wall, m^2, per unit length d. When simulating the seismic impact along the normal to the longitudinal axis of the pipeline, the maximum normal fibre bends σ_M^S and compress σ_N^S stresses are calculated. The total transverse seismic stress (the first component of the effective stress) is determined from the ratio

$$\sigma_I = \sigma_M^S \pm \sigma_N^S. \quad (8)$$

Longitudinal forces $F_k(t)$and bending moments $M_k(t)$ from seismic impact are also determined taking into account the registered three-component accelerograms. The formulas for their definition in this approach take a dynamic form:

$$F_K(t) = \frac{EAv(t)}{\alpha_k V_k} \le F_\tau(T), H, \quad (9)$$

$$M_K(t) = \frac{EJa(t)}{(\beta_k V_k)^2}, H*m, \quad (10)$$

where E – modulus of elasticity of the pipe material, Pa; A – cross-sectional area of the pipe, m^2; $v(t)$ – velocities of soil particles, which are determined by the velosogram, m/s; V_k – velocity of seismic waves; α_k, β_k – characteristic coefficients depending on the type of wave; k – type of seismic wave (1 – longitudinal wave, 2 – transverse wave) [10], [11]; J – moment of inertia of the cross-section of the pipe, $a(t)$ – seismic acceleration, which is determined by the accelerogram, m/s^2; $F_\tau(t) = \lambda_k f_\tau / 4$ – ultimate force of interaction between the soil and the surface of the pipeline, H; $\lambda_k \approx T_0 V_k / 2$ – wavelength, m; T_0 – dominant period of the seismic spectrum, which is determined by the method of Fourier rapid transform to the stationary part of the calculated accelerogram; $f_\tau(t)$ – running friction force, H/m.

The maximum running force of friction between a construction and soil is defined taking into account force of wave influence and coupling of soil with a pipe [11]:

$$f_\tau(t) = \pi D(K_T \rho_0 v(t) V_k + C_0), \quad (11)$$

where D – external diameter of a pipe, m; $K_T = tg\varphi_z$ – coefficient of friction; φ_z – angle of internal friction of the backfill soil, deg; ρ_0 – soil density, kg/m^3; C_0 – adhesion of soil/backfill, Pa.

When modelling the seismic impact along the axis of the pipeline there are calculated:

- longitudinal axial stresses

$$\sigma_l^S = \frac{\min(F_k(t), F_\tau(t))}{A}, \quad (12)$$

- fibre transverse stresses from the bending of the pipeline under the dynamic influence of seismic waves

$$\sigma_t^S = \frac{M_k(t)}{W_{np}}, \quad (13)$$

where Wnp – moment of resistance of profile of a pipe, m^3. Thus, the second component of the effective stresses has the form:

$$\sigma_2 = \sigma_l^S + \sigma_t^S, Pa. \quad (14)$$

Figure 2 shows the dependences of seismic stresses on the time obtained in the simulation of seismic action with a capacity of 8 points for a pipe deepened into the sandstone with a diameter of 1.22 m and a thickness of 18 mm.

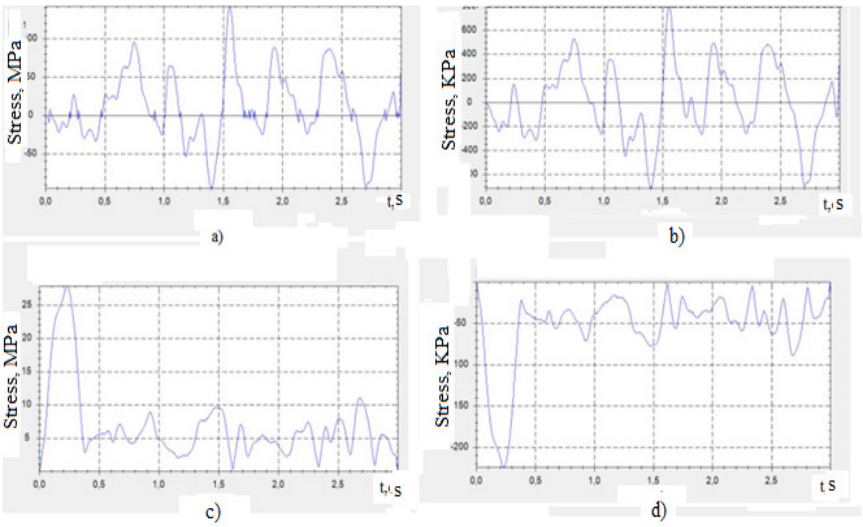

a) axial stresses along the *Z* axis; b) bending stresses along the *Z* axis; b) stresses of the annular bend in the *XY* plane; c) stresses of the annular compression in the *XY* plane

Fig. 2. Dependences of seismic stresses on time.

The impact of seismic influences on the *X, Y* and *Z* axes is determined on the basis of studies of the contribution of transverse impact on the normal to the pipeline axis (on the *X* and *Y* axes) and longitudinal impact (on the *Z* axis) along the pipeline in the overall stress state of the pipeline. The results of study are shown in Fig. 3.

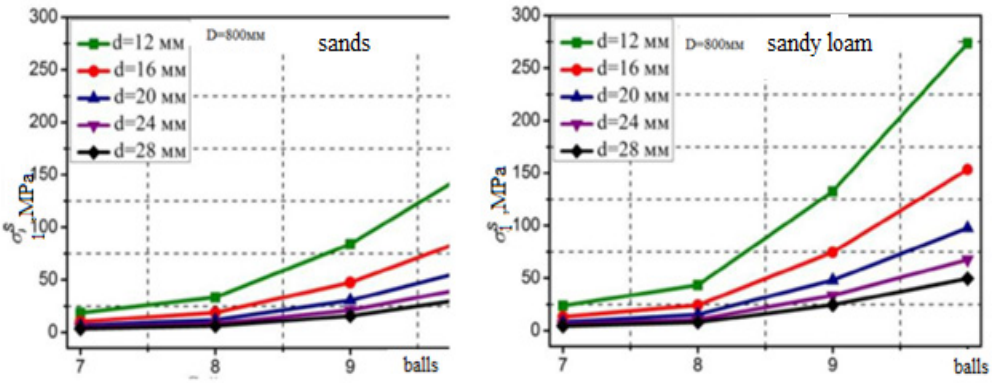

a)

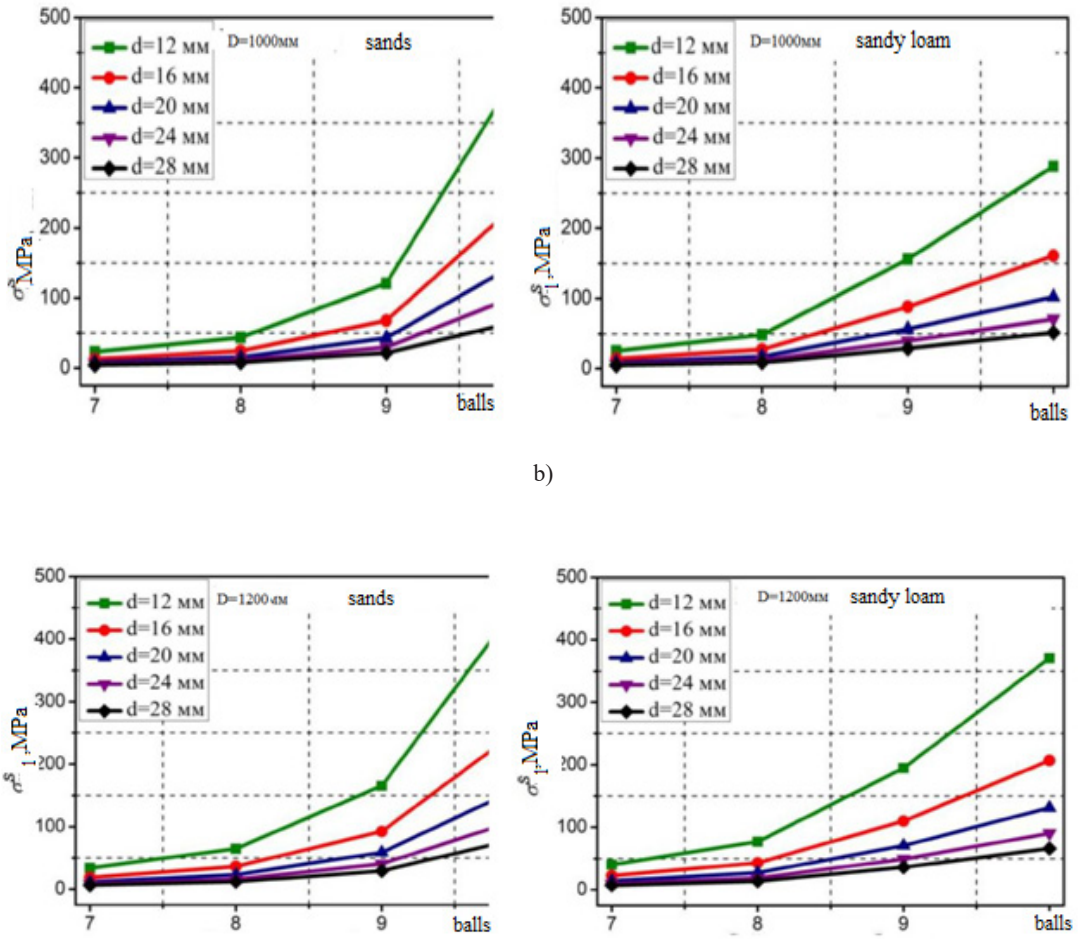

b)

c)

Fig. 3. Dependence of transverse seismic stress on the intensity of seismic impact for deepened in the sand (left) and sandstone (right) pipelines of different thicknesses and diameters – 800 (a), 1000 (b) and 1200 (c) *mm.*

Thus, the value of transverse seismic stresses increases rapidly with increasing intensity of seismic loads. Since the value of spacing resistance for pipes of standard steel grades does not exceed several hundred MPa, taking into account the pressure from the transported product (oil) at an earthquake load of more than 8 points, pipe material goes into an inelastic stage, which can lead to cracks and possible pipeline rupture.

To quantify the contribution of these stresses to the resulting seismic loads, the coefficient K⊥ is introduced, which is determined by the ratio of equivalent seismic stresses to transverse seismic stresses (Table 2).

Table 2. Coefficient K⊥ Taking into Account the Transverse Effect of the Seismic Wave

Wall thickness, *mm*	Pipe diameter, *mm*					
	800		1000		1200	
	Load intensity, point					
	7–8	9–10	7–8	9–10	7–8	9–10
16	1.2	1.25	1.25	1.35	1.40	1.50
20	1,15	1.2	1.2	1.25	1.3	1.40
24	1,10	1.15	1.15	1.2	1.25	1.3
28	1.05	1.10	1.10	1.15	1.2	1.25

As follows from Table 2, depending on the intensity of the earthquake, the diameter of the pipeline, the wall thickness of the pipe and the type of soil, the total stress of the steel material from seismic impact increases by 1.1 ... 1.5 times.

Next, the explosion of a charge of 10 kg of TNT at a depth of 10 m from the earth's surface is considered. It is assumed that the pipeline has a diameter of 1.5 m and is made of steel with the following physical and mechanical characteristics: yield strength 235 H/m^2, Poisson's ratio 0.3, elastic modulus 210 H/m^2, density = 7855 kg/m^3. The depth of laying the pipe is 5 m. Clay is considered as soil.

Figure 4 shows the distribution of stresses in the pipeline from the action of the longitudinal wave, while in the figure their values are indicated by different colours.

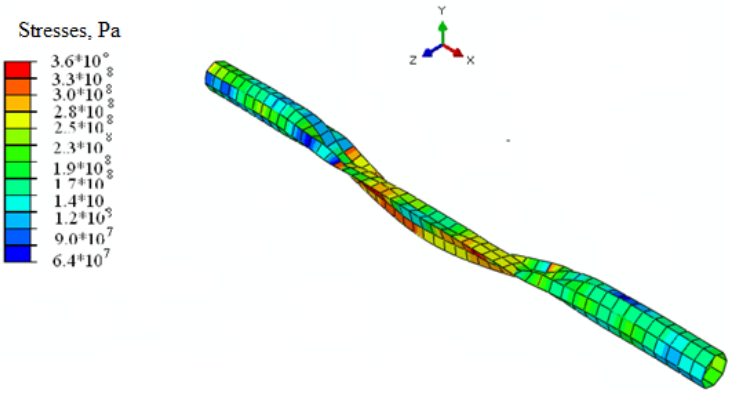

Fig. 4. Stress distribution in a steel pipe with a diameter of 1.5 m under the action of a longitudinal wave during an explosion of a TNT charge weighing 10 kg.

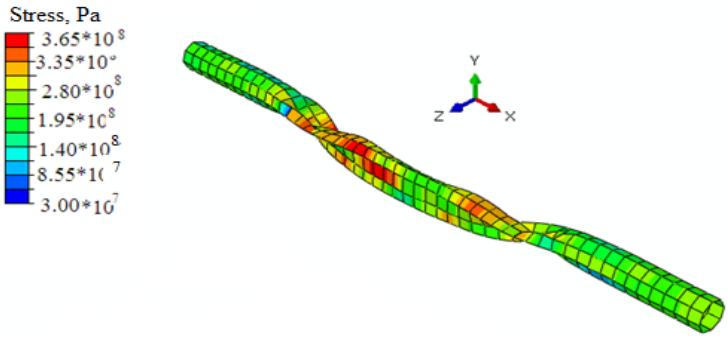

Fig. 5. Stress distribution in a steel pipe with a diameter of 1.5 m under the action of a transverse wave during an explosion of a TNT charge weighing 10 kg.

It is shown that the maximum stress in the pipe reaches a value of 360 MPa, which is significantly more than the steel yield strength.

Figure 5 shows the distribution of stresses in the pipeline from the action of transverse waves.

From the comparison of Figs. 4 and 5, it can be concluded that the transverse wave causes much more damage in the pipe than the longitudinal – the area of damage increases by 1.5 times.

4. CONCLUSIONS

1. The software-calculation module, which implements the model of dynamic strength analysis and allows estimating the magnitude of longitudinal and transverse seismic loads, has been developed within the study.
2. The regularities of the influence of longitudinal and transverse loads from the influence of explosive and seismic waves directed normally to the longitudinal axis of the pipeline on the strength of the pipeline have been revealed.
3. With increasing load intensity and increasing pipe diameter, the voltage changes (increases) as follows: for pipes with a diameter of 800 mm – by 1.05...1.25 times, for pipes with a diameter of 1000 mm – by 1.10...1.35 times, for pipes with a diameter of 1200 mm – by 1.20...1.50 times.
4. The transverse wave causes much more damage in the pipe than the longitudinal one – the area of damage increases by 1.5 times.

REFERENCES

1. Napetvaridze, Sh., Gekhman, A., Spiridonov, B. (1980). *Seismic Resistance of Main Pipelines and Special Structures of the Oil and Gas Industry*. M.: Nauka.
2. Gekhman, A., & Zajnetdinov, H. (1986). *Calculation, Design and Operation of Pipelines in Seismic Regions*. M.: Strojizdat.
3. Remez, N., & Ivanova, I. (2014). Interaction of Seismic Blast Waves with Layered Soil Massif and Underground Pipe. *Herald of NTUU «KPI», Mining, 24,* 27–34.
4. Remez, N., & Krajchuk, S. (2016). *Prediction of Seismic Resistance of Structures during the Explosion of Cylindrical Charges.* Kyiv: Center for Educational Literature.
5. Isaenko, V., Vovk, O. (mol.), Zajchenko, S., Remez, N., & Vovk, O. (2018). Methods of Forecasting and Monitoring of Technologically Dangerous Dynamic Processes in Exempted Territories. Kyiv: NAU.
6. Remez, N., Dychko, A., Kraychuk, S., & Ostapchuk, N. (2018). *Interaction of Seismic Explosive Waves with Underground and Surface Structures.* Resources and Resource-Saving Technologies in Mineral Mining and Processing. Petroșani, Romania: Universitas Publishing, 291–310.
7. Remez, N., Dychko, A., Kraychuk, S., Ostapchuk, N., Yevtieieva, L., Bronitsky, V. (2018). Simulation of Seismic Explosion Waves with Underground Pipe Interaction. *Latvian Journal of Physics and Technical Sciences, 3,* 27–33. DOI: 10.2478/lpts-2018-0011.

8. Remez, N. (2019). Interaction of Blast Waves with Soils and Elements of Techno-Urban Systems. Kyiv: Center for Educational Literature.
9. Andreeva, E. (2007). Calculation Models of an Underground Pipeline under the Influence of Transverse Seismic Effects. *Main and Field Pipelines: Design, Construction, Operation, Repair, 2*, 49–54.
10. Denisov, G., & Lalin, V. (2013). Natural Oscillations of Buried Main Pipelines under Seismic Impact. *Pipeline Transport: Theory and Practice, 4 (38)*, 14–17.
11. Aleksandrov, A., Larionov, V., & Gumerov, R. (2014). Automated Monitoring System for Main Oil Pipelines in Seismically Hazardous Areas. *Herald MGTU im. N.E. Baumana*. *Ser. Mashinostroenie, 5 (98),* 113–126.
12. Abramyan, B., Arutyunyan, N., Birger, I. (1968). *Strength, Stability, Fluctuations*. M.: Mashinostroenie.

sciendo

LATVIAN JOURNAL OF PHYSICS
AND TECHNICAL SCIENCES
2023, N 1

DOI: 10.2478/lpts-2023-0002

THE PHYSICAL PROCESSES OF THE ERRORS ACCUMULATION IN MEASUREMENT SYSTEMS

R. Ramane, P. Trifinovs-Bogdanovs, A. Zhiravetska*

Riga Technical University, 12-k1 Azenes Str.,
Riga, LV-1010, LATVIA
*e-mail: Anastasija.ziravecka@rtu.lv

Nowadays autonomous measurement systems are applied for the determination of the cinematic parameters of object motion. The principle of operation of such systems is based on the measurement of the object motion acceleration with the further integration of the accelerometer's signal. These measurement systems are called inertial systems. Platform-less inertial systems are widely used for these purposes. Their specific property is an installation of the primary information sensors directly on the constructive elements of the object case. The inertial measurement systems have also a negative feature to accumulate constantly the errors of the system.

Keywords: Block diagram, correction, error accumulation, inertia, integrator, platform-less.

1. INTRODUCTION

Modern platform-less inertial systems have a complicated structural multicomponent block diagram with a large number of links among the elements. Inertial systems determine the parameters of the motion in 3D space [1], [2]. Therefore, they have three channels (Fig. 1). This paper is devoted to the analysis of the errors accumulation by a platform-less inertial system. The errors are formed in its structure [3]–[5]. The structural block diagram of the inertial system is separated into comparatively simple functional parts. Thus, the accumulation of the errors was investigated in its separate parts [6].

Decision chains are an inertial system core; they contain an integrator of speed and an integrator of distance connected in series. Modern platform-less inertial systems contain also chains of accelerometer's self-correction and chains of calculation of the object motion angles (Fig. 1). The cor-

rection chains together with decision chains make closed loops. The feedback in these loops is the correction chains [7]–[10].

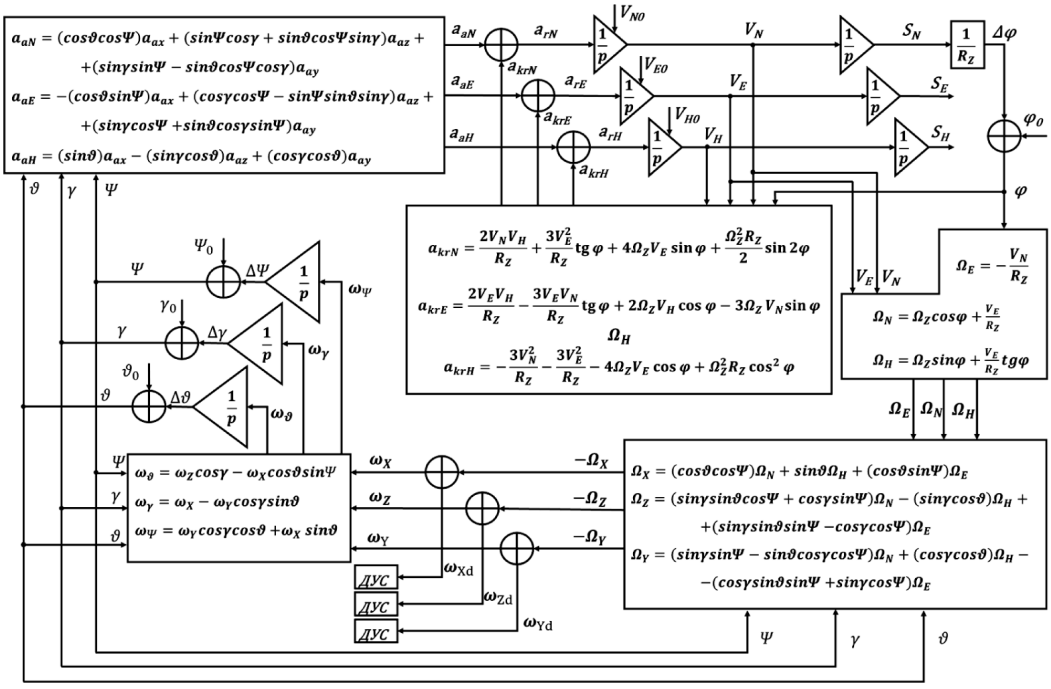

Fig. 1. Structural block diagram of the measurements of the cinematic parameters of a moving object.

2. ANALYSIS OF THE SYSTEM UNDER CONSIDERATION

1. The decision chain is a functional element of the principal realisation: $V_i = \int a_{ai}\, dt$, $S_i = \int V_i\, dt$. However, for the errors of the primary information sensors Δa_{ai} the decision chain is a chain of forming errors for the whole system $\Delta V_i = \int \Delta a_{ai}\, dt$, $\Delta S_i = \int \Delta V_i\, dt$. Forming of the errors is a side effect of the inertial system structure operation. The basic functional chain of the inertial system – the decision chain – forms the errors ΔV_i and ΔS_i increasing (accumulated) in time.
2. The circuits of self-correction of the inertial system (closed loops with feedback) significantly influence the accumulation of errors by the inertial system. The development of the errors in each separate functional chain has been analysed under the condition when there is a constant error Δer at the input of the chain.

2.a. Single integrator loop with parallel feedbacks. A part of the structural block diagram has been investigated when one integrator has two parallel feedback loops with different signs and values of transfer factors (Fig. 2, -к, +к2).

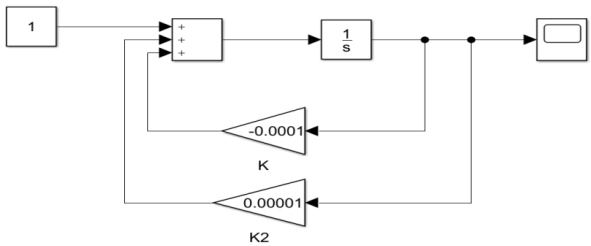

Fig. 2. Model of a part of the measurement of the cinematic parameters. Single-integrator loop with the feedback.

The graphs in Fig. 3 demonstrate the results of modelling of the operation of two variants of single-integrator loop (Fig. 3a, -K=-0.0001 and +K2=0.00001, and Fig. 3b, -K=-0.0001 and +K2=0.001).

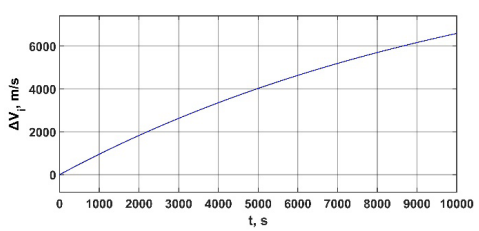

Fig. 3a.

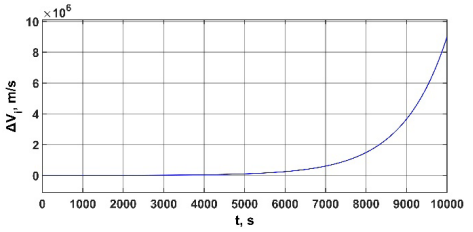

Fig. 3b.

Fig. 3. Accumulation of the error of speed in the single-integrator loop with different transfer factors in the feedback (Fig. 3a. -K=-0.0001 and +K2=0.00001; Fig. 3b.-K=-0.0001 and +K2=0.001).

Quality of the structure with two feedback loops is determined by the feedback with a higher value of transfer factor. If the transfer factor of the negative feedback -K has higher value, then the structure is stable (Fig. 3a), and the error of the loop is stabilised at a particular level. If the transfer factor of the positive feedback +K2 has higher value, then the structure is unstable (Fig. 3b) and the error ΔV_i is increasing with time. Analysis of the transient process shows that the value of the error ΔV_i depends on the value and sign of the total coefficient of feedback circuits.

$$\Delta V_i(t) = \frac{\Delta a_{ai}}{K_2 - K}\left(1 - e^{(k_2 - k)t}\right) \quad (1)$$

2b. Double-Integrator Loop with Parallel Chains of Feedback

In the structure of double-integrator loop the feedback chains cover two integrators. These feedback chains realise different functions and therefore have different transfer factors (with different signs and values (Fig. 4)).

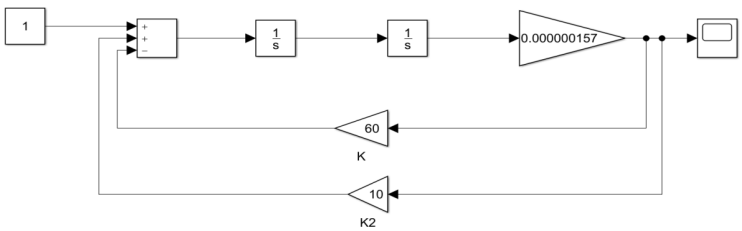

Fig. 4. Double-integrator loop of the structural block scheme of the cinematic parameter measurement.

Figure 5a shows the time diagram of the error Δ φ variations, when one loop (K=-K=60) forms negative feedback, but the other loop (K2=+K2=10) forms positive feedback. Figure 5b shows the time diagram of the error Δ φ variations, when -K=60 a +K2=100.

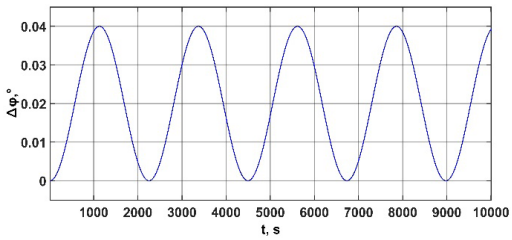

Fig. 5a.

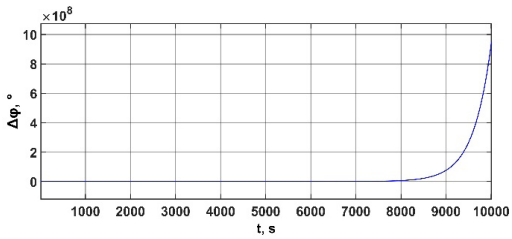

Fig. 5b.

Fig. 5. Time diagrams of the variations of the double-integrator loop latitude angle error with different transfer factors in the feedback (Fig. 5a. -(K=-K=60 and +K2=10; Fig. 5b. -K=-60 and +K2=100).

The quality of the structure of the double-integrator loop with the parallel feedback chains is determined by the value and sign of the total transfer factor of the parallel feedback chains (the same like in the single-integrator loop (Fig. 2)). If the total transfer factor is negative, the system is stable (Fig. 5a). The transient process and value of error Δ φ have the properties of oscillations (Fig. 5a). If the total transfer factor of the parallel feedback chains is positive, then the system is unstable. The error of the system Δ φ will be accumulated with time (Fig. 5b).

2c. Double-Integrator Loop Formed by the Structural Elements of Different Channels

The structure of an inertial system has cross links among the channels. It results in specific (combined) loops containing elements from different channels of the system (Fig. 6).

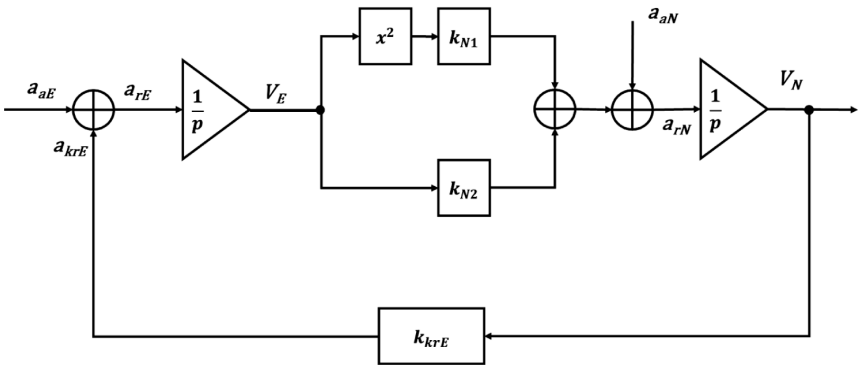

Fig. 6. Block diagram of the double-integrator combined loop.

Two different signals form the sensors of primary information – Δ a_N и Δ a_E – will be supplied also into this complex double-integrator loop. Thus, the error from one channel will be supplied into another forming the cross links among the channels in the structure of the measurement system.

The operation of the combined double-integrator loop with multichannel elements was modelled for the case of the eastern

channel accelerometer's error existence Δa_E and if the feedback is negative with two transfer factors (Fig. 7, K_{krE} = - 0.0002761, K_{krE}= - 0.2761). The modelling results are demonstrated in Fig. 7a and 7b.

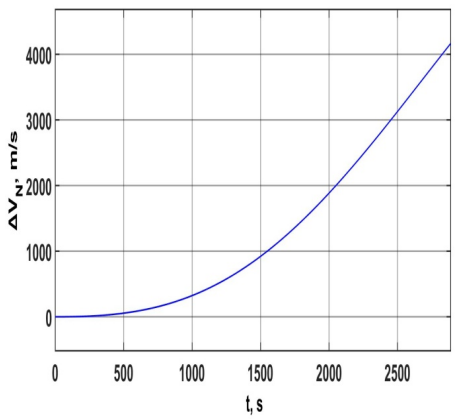

Fig. 7a.

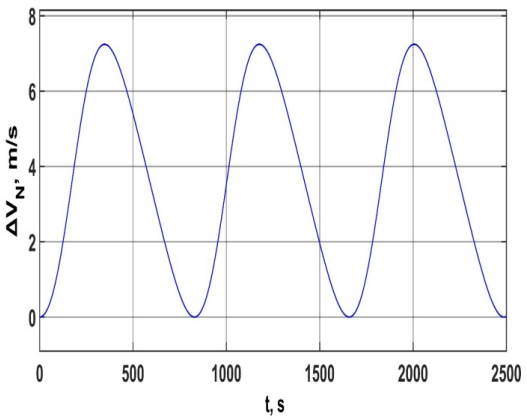

Fig. 7b.

Fig. 7. Time diagrams of the variations of the double-integrator loop velocity error with different transfer factors in the negative feedback (Fig. 7a. K_{krE} = - 0.0002761; Fig. 7b. K_{krE}= - 0.2761).

If the feedback of the double-integrator loop is positive with two values of the transfer factor (Fig. 6, K_{krE}= 0.0002761, and K_{krE}= 0.02761), the output signal of the velocity integrator of the northern channel ΔV_N is a growing function (Fig. 8a, Fig. 8b).

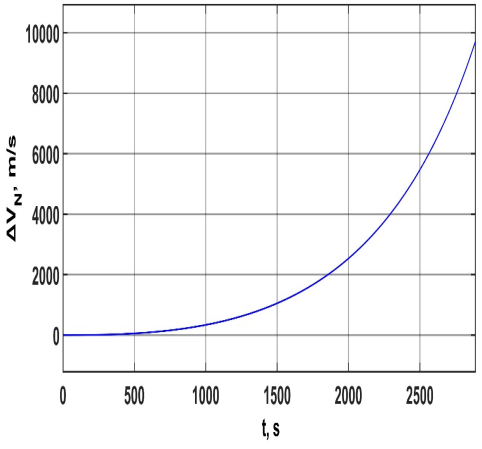

Fig. 8a.

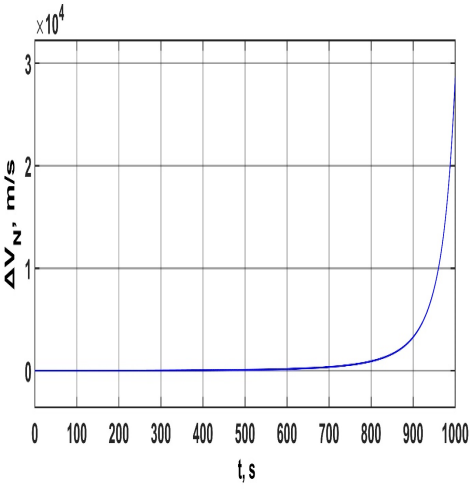

Fig. 8b.

Fig. 8. Time diagrams of the variations of the combined double-integrator loop velocity error with different transfer factors in the positive feedback chains (Fig. 8a. K_{krE} = 0.0002761; Fig. 8b. K_{krE}= 0.2761)

Analysing the operation of the double-integrator loop supplying the error signal Δa_E onto its input a mathematical expression is obtained for the transient process. If the feedback is negative then the variation of the loop error ΔV_N is changed and stabilised around some value, which depends on the values of the error Δa_E and the value of the transfer factor K_{krE}.

$$\Delta V_N(t) = \frac{\Delta aE}{KkrE}(1 - \cos\sqrt{KkrE}\ t). \quad (2)$$

If the feedback is positive then the variation of the loop error ΔV_N is continuously increasing in time.

$$\Delta V_N(t) = \frac{\Delta aE}{KkrE}(1 - ch\sqrt{KkrE}\ t). \quad (3)$$

The speed of the error increasing ΔV_N depends on the values of error Δa_E and feedback factor K_{krE}.

3. DISCUSSION

The combined double-integrator loop can have another variant of operation when the error is supplied to the middle point of the loop (Fig. 6, the error of the northern channel accelerometer Δa_N). Modelling of this structure resulted in a similar case like the latter, when error Δa_E was submitted onto the loop input. If the feedback is negative then the variation of the loop error ΔV_N is changed and stabilised around some value which depends on the values of the error Δa_N and the value of the transfer factor K_{krE}.

$$\Delta V_N(t) = \Delta a_N \cos\sqrt{KkrE}\ t. \quad (4)$$

If the feedback is positive then the variation of the loop error ΔV_N is continuously increasing in time.

$$\Delta V_N(t) = \Delta a_N ch\sqrt{KkrE}\ t. \quad (5)$$

Difference in the input points of the error into the double-integrator loop results in the difference of the quantitative characteristics of the loop error. When the error is supplied to the loop input the value of the transfer factor of the feedback K_{krE} impacts the amplitude and cycle of the loop error variation. The less is the transfer factor K_{krE}, the higher is the loop error ΔV_N, the larger is the cycle of the error ΔV_N variation. When the error is supplied to the middle point of the loop, the value of the feedback transfer factor K_{krE} impacts the value of the cycle of the loop error variation.

Single-integrator and double-integrator loops in most of the cases are the structural elements in the chains of accelerometer's signal correction. These loops can decrease the accumulated error of the inertial system's decision chain (in the case of negative feedback in the circuits).

3. Three-integrator loop. Platform-less inertial system contains the self-correction chains for calculation of the object motion angles. It results in new closed loops in the system (Fig. 9).

A three-integrator loop with feedback exists (Fig. 9. ,K_2, K_3, the only closed is $Sl_{1\varphi}$,). The specific property of this functional structure is three integrators connected in series. A double-integrator loop composed of two integrators of the three-integrator loop is inside this loop (Fig. 9. K_1, K_4, the only closed is Sl_{2V}). Two errors Δa_N and $\Delta \Omega z$ are supplied into the loops from two sensors of the primary information.

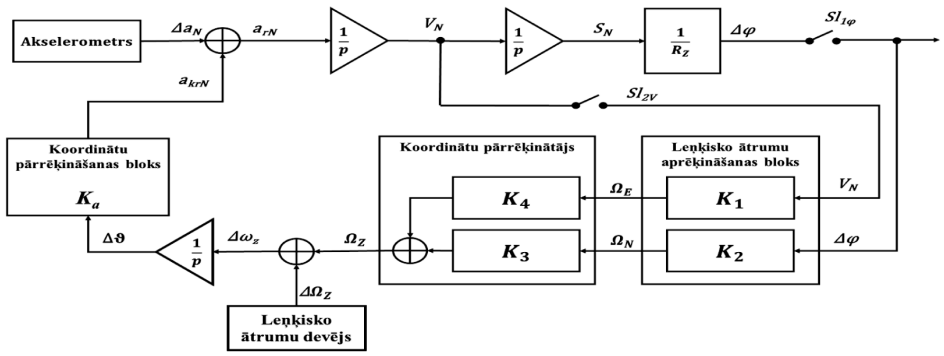

Fig. 9. Self-correction chains for calculation of the object motion angles

The paper contains modelling of operation of different variants of the three-integrator loop.

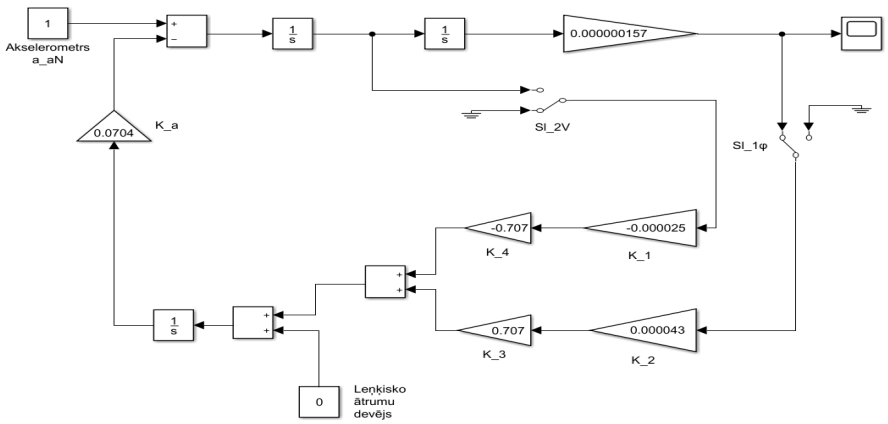

Fig. 10. Modelling of operation of three-integrator loop.

3a. Two values of the transfer factor of negative feedback were supplied at the input of the loop of the accelerometer's error Δa_N K_2 =-0.000043 (Fig. 11a.) and K_2= - 0.43 (Fig. 11b.).

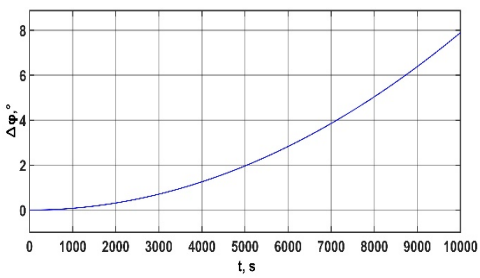

Fig. 11a.

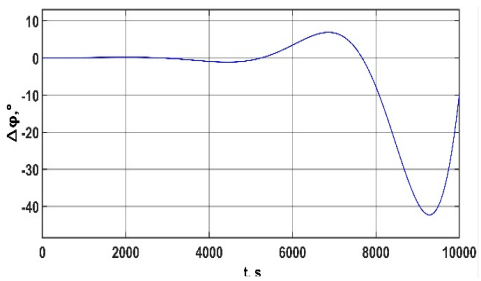

Fig. 11b.

Fig. 11. Diagrams of error variation for the latitude angle of the three-integrator loop with different transfer factors in feedback (Fig. 11a. K_2 =-0.000043; Fig. 11b. - K_2 =-0.43).

According to Fig. 11a and b, with the existence of the accelerometer's error Δa_N the three-integrator loop with negative feedback is an unstable structure. The loop error is increasing with time.

3.b. Modelling of the operation of the three-integrator loop with positive feedback and the same values of factors K_2 (K_2 = 0.000043 (Fig. 12a) and K_2= 0.43 (Fig. 12b).

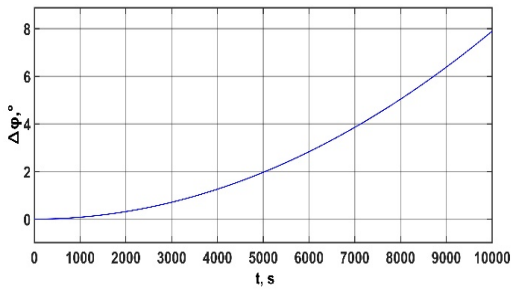

Fig. 12a.

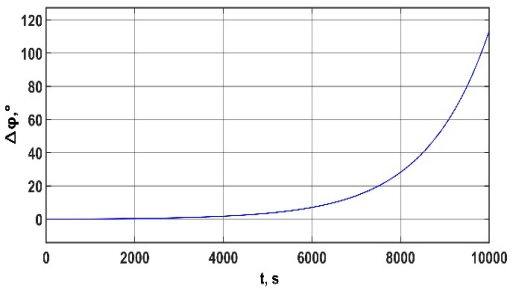

Fig. 12b.

Fig. 12. Error variation for the latitude angle of three-integrator loop with different transfer factors in the feedback (Fig. 12a, K_2 = 0.000043; Fig. 12b., K_2 =-0.43).

It is obvious from Fig. 12a and 12b that with the accelerometer's error Δa_N the three-integrator loop with positive feedback is an unstable structure and the loop error is accumulated with time.

4a. Modelling of the three-integrator loop with the error of the angular velocity sensor supplied to the input of the loop $\Delta \Omega z$ (Fig. 10). This variant was realized with two values of the transfer factor of the negative feedback K_2 =-0.000043 (Fig. 13a) and K_2= - 0.43 (Fig. 13b).

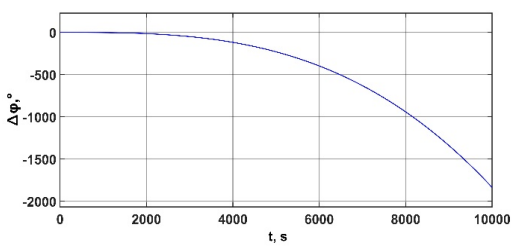

Fig. 13a.

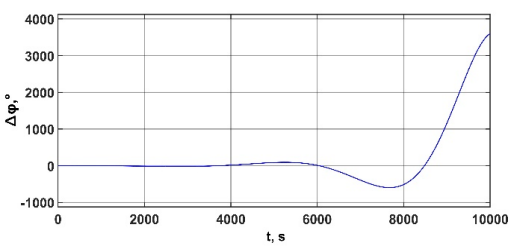

Fig. 13b.

Fig. 13. Diagrams of variations of the latitude angle error in three-integrator loop with different transfer factors in the feedback (Fig. 13a, K_2 = -0.000043; Fig. 13b,. K_2 =-0.43).

The diagrams in Fig. 13a and Fig. 13b demonstrate that at the presence of error from the speed sensor $\Delta \Omega z$ the three-integrator loop with negative feedback is an unstable structure. The error of the loop is increased with time.

4b. Three-integrator loop with positive feedback. The input of the loop is supplied with the error from speed sensor $\Delta \Omega z$. The transfer factor of the feedback is K_2 =0.000043 (Fig. 14a) and K_2= 0.43 (Fig. 14b).

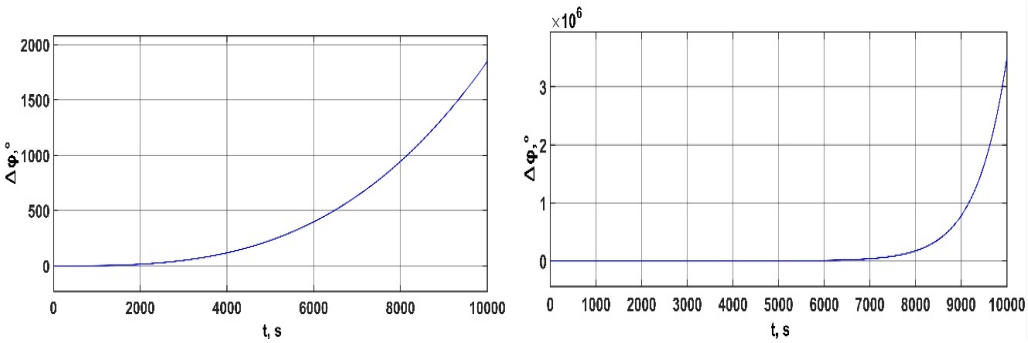

Fig. 14a. Fig. 14b.

Fig. 14. Diagrams of variations of the latitude angle error in three-integrator loop with different transfer factors in the feedback (Fig. 14a. $K_2 = 0.000043$; Fig. 14b. $K_2 = 0.43$).

The diagrams in Fig. 14a and Fig. 14b. demonstrate that at the presence of error from the speed sensor the three-integrator loop with positive feedback has an unstable structure.

The processes in the larger three-integrator feedback chain are unstable at both positive and negative feedback and different transfer factors of the feedback.

The mathematical descriptions of the error accumulation process in three-integrator loop (Fig. 10) for the case of negative feedback and presence of the error from the operation of the sensor of primary information by the angular velocity $\Delta \Omega z$ of the inertial system are the following:

$$\Delta S_i(t) = -\frac{k_a}{3a^2}\{ e^{-at} - e^{at/2}[\cos\frac{a\sqrt{3}}{2}t - \sqrt{3}\sin\frac{a\sqrt{3}}{2}t\ ]\ \}\ \Delta \Omega z\ (t), \quad (6)$$

where – $a = \sqrt[3]{K_a K_2 K_3 K_\varphi}$

For the case of negative feedback and error of the accelerometer operation Δa (Fig. 10):

$$\Delta S_i(t) = \frac{1}{3a^2}\int \{ e^{-at} - e^{at/2}(\cos\frac{a\sqrt{3}}{2}t - \sqrt{3}\sin\frac{a\sqrt{3}}{2}t\ )\ ]\ dt\ \}\ \Delta a(t). \quad (7)$$

The expressions show that initially the transient process $\Delta S_i(t)$ is developing relatively slowly (increasing) due to the influence of the stabilising factor. After some time a destabilizing factor will be influencing the process resulting in the continuous increase of the speed of the output value $\Delta S_i(t)$ increasing in the measurement system.

5. Double-integrator loop in the self-correction system of calculation of the angles of the object motion (Fig. 10). This type of double-integrator loop of the angle self-correction quantitatively has the same transient process of the error variation like that of accelerometer self-correction (position 2, Fig.4) for the case when the loop input is sup-

plied with accelerometer error Δa_N. The results of the error development are significantly changed when the error of the angular velocity sensor $\Delta \Omega z$ is supplied onto the input of double-integrator loop of angular self-correction operating together with three-integrator.

5a. Double-integrator loop of the angular self-correction with negative feedback. The input of the loop is supplied with the error from the angular velocity sensor $\Delta\omega$ with two variants of transfer factors of the feedback K_1=-0.000025 (Fig. 15a) and K_1= - 0.0025 (Fig. 15b).

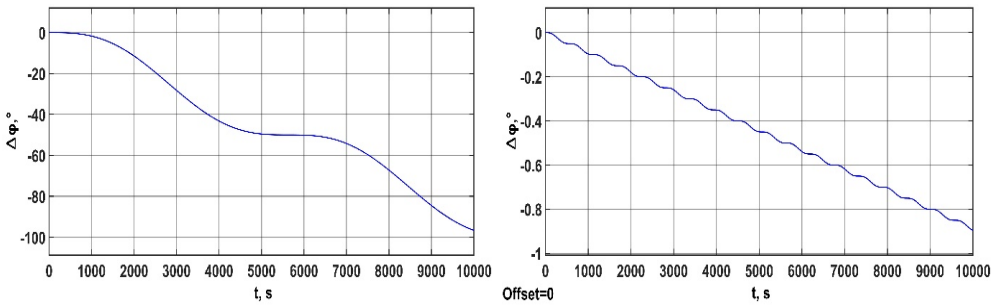

Fig.15a. Fig. 15b.

Fig. 15. Diagrams of the error variations for the latitude angle of double-integrator loop with different transfer factors in feedback (Fig. 15a, K_1=-0.000025; Fig. 15b, K_1 = - 0.0025).

The diagrams show that supplying the error $\Delta\omega$ to the input of double-integrator loop of the angular self-correction with negative feedback, the output signal of the loop $\Delta\varphi$ is increased with time and the system is unstable.

5b. Double-integrator loop of angular velocity self-correction with positive feedback (K_1= 0.000025 and K_1= 0.0025) supplying an error from the angular velocity sensor $\Delta\omega$ onto the loop input (Fig. 16a and Fig. 16b).

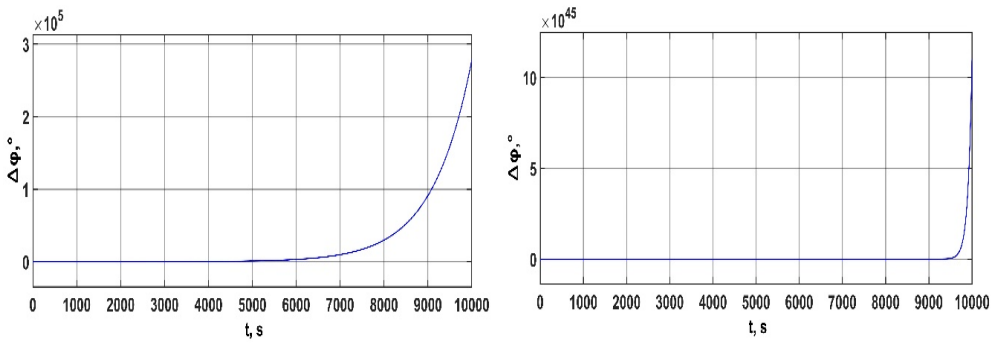

Fig. 16a. Fig. 16b.

Fig. 16. Diagrams of the error variations for the latitude angle of double-integrator loop with different transfer factors in feedback (Fig. 15a, K_1= 0.000025; Fig. 15b, K_1 = 0.0025).

The diagrams demonstrate that in the case of the error of angular velocity at the input double-integrator loop with positive feedback the output signal of the loop

is increased with time and the structure is operating in an unstable regime. Thus, the error input point from the angular velocity sensor $\Delta\omega$ in the double-integrator loop of angular self-correction is critical. The input point of the accelerometer error Δa_N into double-integrator loop is critical only in the case if the feedback of the loop is positive. The self-correction chains for calculations of the object motion angles give a negative effect in the process of decreasing of the errors in inertial system.

All mentioned above demonstrate the secondary consequences of the application of self-correction chains. The application of the functional self-correction chains positively affects the optimization of the measurement (inertial) system operation. However, the same functional chains simultaneously form the errors of the measurement system. In this situation their influence is mostly negative, resulting in increasing of the system's error. The self-correction chains influence negatively the calculation of the object angles. In this case the errors could be reduced decreasing the errors of the sensors of the primary information. However, anyway the dynamics of the system's errors variation (their accumulation with time) is determined by the structure of the decision chains and chains of self-correction.

4. CONCLUSIONS

Application of correction of some elements of an inertial system results in existence of additional functional chains in the system structure that significantly influence the values and variations of the system errors. When the integrators are covered by the positive and negative feedback chains the block diagram of the inertial system is getting additional closed loops. The correction of the accelerometer's signals results in closed single or double loops in the decision chains of the inertial system. The positive feedback in these circuits results in a continuous increase (accumulation) of errors of the system with time. The negative feedback in turn results in stabilisation of the system errors according to a particular level, which is signalling about the system stability by the error accumulation. Calculation of the angular positions of a moving object results in the formation of a large, three-integrator, closed loop. Such a structural scheme will constantly accumulate the error with time at the presence of both positive and negative feedback chains. Therefore, the introduction of the circuits of the moving object's angle calculation into the structure of the inertial system results in instability by the error accumulation.

REFERENCES

1. Zhiravetska, A., Trifonov-Bogdanov, P., & Shestakov, V. (2012). Mechanisms of Error Development in Inertial Navigation Systems, *Aviation*, *16* (2) 33–37.
2. Britting, K. (2010). *Inertial Navigation Systems Analysis*. London: Artech House Print.
3. Lawrence, A. (2001). *Modern Inertial Technology.* Berlin: Springer.
4. Wrigley, W., Hollister, W., & Denhard, W. (1969). *Gyroscopic Theory, Design and Instrumentation*. Cambridge: M.I.T. Press.

5. Grewal, M.S., Weill, L.R., & Andrews, A.P. (2004). *Global Positioning Systems, Inertial Navigation and Integration*. NJ: Wiley.
6. Vaisgant, I. (1984). *Inertial Navigation Systems Structure Principles*. Saint Petersburg: LETI.
7. Matvejev, V. (2012). *Inertial Navigation Systems*. Tula: TulGu.
8. Moir, I., & Seabridge, A. (2006). *Civil Avionics Systems*. Wiley-Blackwell.
9. Trifonovs-Bogdanovs, P., Žiravecka, A., Trifonova-Bogdanova, T., & Mamay, K. (2017). Structural Correction of Inertial System Circuit. *Transport and Aerospace Engineering*, *4*, 46–52. ISSN 2255-968X. e-ISSN 2255-9876.
10. Method for Structural Correction of Inertial Navigation System, Republic of Latvia. (2012). Patent – 14487. ISSN 1691-5968.

sciendo

LATVIAN JOURNAL OF PHYSICS
AND TECHNICAL SCIENCES
2023, N 1

DOI: 10.2478/lpts-2023-0003

GREEN AND SUSTAINABLE HYDROGEN IN EMERGING EUROPEAN SMART ENERGY FRAMEWORK

L. Jansons[1,2], L. Zemite[1]*, N. Zeltins[1], I. Geipele[2], A. Backurs[3]

[1]Riga Technical University,
Faculty of Electrical and Environmental Engineering,
Institute of Power Engineering
12-1 Azenes Str., Riga, LV-1048, LATVIA
[2]Riga Technical University,
Faculty of Engineering Economics and Management,
Institute of the Civil Engineering and Real Estate Economics,
6 Kalnciema Str. 210, Riga, LV-1048, LATVIA
[3]Latvian Hydrogen Association
Akademijas laukums 1, Riga, LV-1050, LATVIA
*e-mail: laila.zemite@rtu.lv

Green and sustainable hydrogen has a major role in moving towards decarbonization of energy, providing viable solutions in all most challenging sectors of the national economies. It would penetrate practically all sectors of economic activity, such as long-haul transport, steel and chemical industries, power generation and energy storage. Green and sustainable hydrogen cost competitiveness is also closely linked to developments of large-scale renewable energy sources (in case of green hydrogen; *hereinafter* – RES) and further commercialization of carbon dioxide (in case of sustainable hydrogen produced from natural gas; *hereinafter* – CO_2) capture and storage (*hereinafter* – CCS) technologies.

In the European Union (*hereinafter* – EU), sustainable and especially green hydrogen is gaining strong political and business momentum, emerging as one of major components in governments' net zero plans within the European Green Deal and beyond. Being extremely versatile both in production and consumption sides, it is light, storable, has high energy content per unit mass and can be readily produced at an industrial scale. The key challenge comes from the fact that hydrogen is the lightest known chemical element and so has a low energy density per unit of volume, making some forms of long-distance transportation and storage complex and costly.

In this paper, green and sustainable hydrogen is reviewed as a vital part of emerging European smart energy framework, which could contribute significantly to economy decarbonization agenda of the EU and Latvia in both in short- and mid-term perspective.

Keywords: *Decarbonization, green hydrogen, smart energy systems, sustainable hydrogen.*

1. INTRODUCTION

Use of hydrogen in the energy sector has a long history, which begun with the first internal combustion engines over two centuries ago. Currently, it forms an integral part of the modern chemical and refining industry. Hydrogen is light, storable, energy-dense, and produces no direct emissions of greenhouse gases (*hereinafter* – GHG). For hydrogen to make a significant impact on the EU energy transitions, which is tended to illuminate around 90 % of all EU's GHG emissions by 2050 [1], it needs to be adopted in sectors where it is almost completely absent at the moment. Such sectors include, but are not limited to transport, buildings, power generation and direct gaseous fuel supplies, while introducing renewable gases (*hereinafter* – RGs) to conventional natural gas transmission and distribution networks [2].

Despite characteristics that make hydrogen unique for energy applications, in its pure form hydrogen has highly reactive properties with high combustibility and very low energy density. It means that this gas requires careful handling, transport and distribution as well as typically high-pressure systems for use in final applications. The main characteristics of hydrogen in comparison with the other form of gaseous fuel – methane (the main ingredient of natural gas or biomethane) are shown in Table 1.

Table 1. The Main Characteristics of Hydrogen and Methane

Properties	Hydrogen	Methane (natural gas)
Self-ignition temperature (°C)	585	540
Flame temperature (°C)	2045	1875
Ignition limits in air (vol. %)	4-75	5.3-15
Minimal ignition energy (mWs)	0.02	0.29
Flame propagation in air (m s-1)	2.65	0.4
Diffusion coefficient in air (cm2 s-1)	0.61	0.16
Toxicity	-	-

The International Energy Agency (*hereinafter* – IEA) estimates that the demand for hydrogen in its pure form currently is around 70 million tonnes per annum (*hereinafter* – Mtpa) with the majority or over 90 % of it originated in oil refining industry and ammonia production for the fertilizers manufacturing industry [1]. If demand for hydrogen in pure and non-pure forms is combined, the total demand, according to The International Renewable Energy Agency, can exceed 100 Mtpa, with the actual demand in 2021 standing at 94 Mtpa [3]. All of it was produced almost exclusively from fossil fuels, such as natural gas and coal, releasing around 900 Mt of CO_2 into the atmosphere. The average global percentage of hydrogen produced from natural gas stands for more than 70 % [4]. Today, 6 % of global natural gas and 2 %

of global coal resources go into hydrogen production [3].

At the same time, by mid-2021, a global capacity of electrolysers, which are needed to produce green hydrogen, reached about 300 megawatts (*hereinafter* – MW). At the end of 2022, according to some estimates [5], it could already reach 1.4 giga-watts (*hereinafter* – GW), but by 2026 – even 8.5 GW [6]. From 2020 to 2021, the hydrogen production market was valued at 130 billion US dollars. It is estimated to grow up to 9.2 % per year through 2030 [7].

Source: GlobalData Thematic Research

Fig. 1. Global electrolyser capacity (GW), 2022.

Around 522 projects, 43 of which at GW scale, are currently under development, and could bring global electrolyser capacity up to 54 GW by the end of this decade. Another 40 projects accounting for more than 35 GW of electrolyser capacity are at the early stages of development. The majority of hydrogen activity, with 261 projects [8], is located in Europe. Many European countries have been investing to find non-carbon intensive alternatives for industrial and transportation usage in line with the EU Green Deal and an effort to strengthen the local fuel value chain.

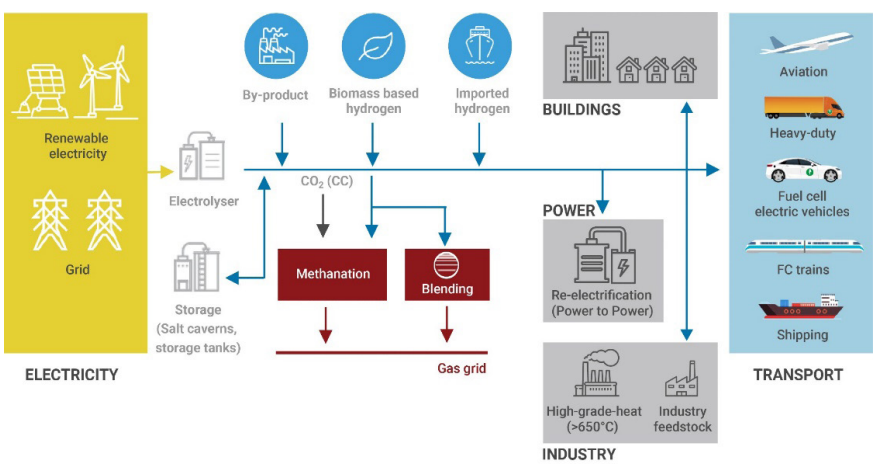

Source: IRENA

Fig. 2. An example of green hydrogen production, supply and consumption chain.

As for today, the main green hydrogen source technologies are alkaline water electrolysis, proton-exchange membrane electrolysis, and solid oxide electrolysis, with the latter being in the research and first-trial phase [9]. If all planned projects are completed, global green hydrogen supply could reach more than 8 Mt by 2030, but this is still well below the 80 Mt required in the way to net zero CO_2 emissions by 2050, or 70Mt short of the most conservative EU energy decarbonisation target for the same date [3].

The installed capacity growth, coupled with growth in demand, would require rather massive energy input. For instance, 22 000 terawatt-hours (*hereinafter* – TWh) of RES electricity to produce 500 million tons of green hydrogen per year are needed, and the parallels of the hydrogen value chain to that of the fossil fuels (with upstream, midstream, and downstream elements) can be drawn. To date, only a few green hydrogen projects have been successfully brought to market. According to *PricewaterhouseCoopers*, most green hydrogen projects under construction and in operation are at the pre-commercial phase with electrolyser capacity less than 50 MW [10]. While some proposed plants are of 100 MW capacity or more, they remain small compared to fossil fuel counterparts. In addition, green hydrogen projects pose some risks that challenge traditional project financing: relative immaturity of the technology, segmentation and fragmentation of energy input, challenges of production and transformation, challenges of storage and long-distance transportation and limited consumer accessibility [4], [11], [12].

In the EU, the European Commission's (hereinafter – EC) long-term energy and economy decarbonization path includes stimulus for wider adoption of low carbon technologies, including hydrogen. In 2020, the EU hydrogen strategy for a climate-neutral Europe was adopted [13], with many EU countries presenting their own national hydrogen strategies soon after. Even those countries that are currently lacking such strategies as separate policy planning document are integrating the green hydrogen component into their national energy and climate plans (hereinafter – NECPs) [14]. Globally, by 2021, nine governments have already adopted a hydrogen strategy. Thus, the total number of governments that have committed to adopt hydrogen as a clean energy vector in their energy agendas has increased to 26 [15].

For instance, the EC has set up a "Hydrogen Energy Network", an informal group of experts composed of representatives from the ministries in charge of energy policy in the EU Member States, aiming to support national authorities to develop hydrogen technology opportunities. The countries have signed the declaration on the "Hydrogen Initiative", which promotes cooperation on sustainable hydrogen technologies. "Hydrogen Europe" is a leading European association promoting the development of hydrogen as the enabler of net zero society. Currently, it has over 160 industrial members across Europe [16]. Initiatives include the Fuel Cells and Hydrogen Joint Undertaking (*hereinafter* – FCH JU), a public-private partnership with the EC that drives a funding stream of 1.33 billion euro (*hereinafter* – EUR) under the EU Horizon 2020 Program, with the aim of accelerating the market adoption of hydrogen technologies in energy, industry and transport [17].

However, strong green hydrogen backing strategies can only work as part of a smart energy framework or all-inclusive, innovative energy supply agenda. It means that not only the current EU energy distribution grids, but also transmission systems need to transform into unified, fully flex-

ible and remotely manageable frameworks with new technologies such as smart solar, energy storage, smart metering and smart gas management. These components would help form self-sufficient and synergetic energy ecosystem, where green and sustainable hydrogen would also play an important role not only in industrial applications, but also in transport and, to some extent, in household energy supply. Low-volume energy consumers in this framework would become prosumers and actively participate in the energy market, and their behaviour would have a major impact on the entire energy ecosystem. A unified smart energy framework will enable consumers to transform into individual energy "uploaders and downloaders", while keeping the overall, differentiated energy system safe, reliable, and affordable and ensuring the system develops toward increasing sustainability [18].

Such a framework building approach is also applicable to RGs like biomethane, sustainable and green hydrogen, which in future would be present in almost all segments of the EU energy sector, and need to be adequately integrated into the new energy ecosystems.

2. A HYDROGEN PATHWAY TO SMART GAS DISTRIBUTION

In order to increase not only production of sustainable and green hydrogen, but also boost its use across the energy sector, the smart energy systems – new, digitalized and sectorally synergized energy architecture solutions and frameworks – are needed to be implemented. The smart energy system concept in most cases addresses cost-effective, highly digitalized RES-only based systems [19], with an inclusion of energy efficiency and infrastructure enhancement efforts. However, not all interpretations of the concept are exclusively dealing with RES, as smart energy systems often are identified with maximally diversified, sustainable energy systems, where some forms of fossil fuel and, especially, energy storage, can or must be present [20].

As green and sustainable hydrogen is RG, smart energy systems should include gas supply chain elements both at the level of transportation and distribution, and storage. In some infrastructure-oriented cases of smart energy system concept interpretation, as shown in Fig. 3, neither fossil nor RES take a central stage – on the contrary, smart grids and storage capacities take the lead [21].

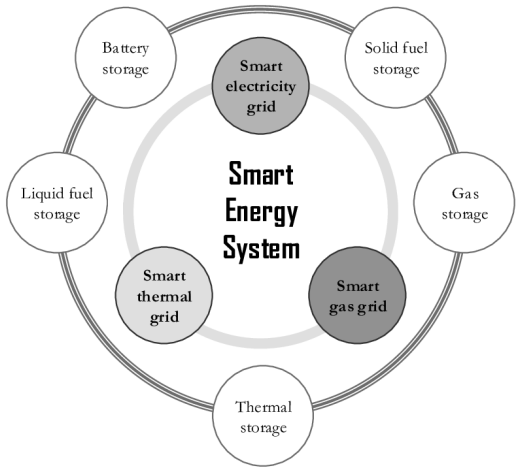

Fig. 3. Principial scheme of grid and storage centered (infrastructure-oriented) smart energy system [21].

As opposed to the smart grid concept, which first and foremost took a sole focus on the electricity sector [22], the smart energy systems approach includes the entire energy generation and consumption spectrum in its identification of suitable energy

infrastructure designs and operation strategies. Focusing only on the smart electricity grid often leads to the definition of transmission lines, flexible electricity demands, and electricity storage as the primary means of dealing with the integration of fluctuating RES. However, these measures alone are neither very effective nor cost-efficient considering the nature of large, variable energy sources. The most effective and least-costly solutions are to be found when the electricity sector is combined with the heating and cooling sectors, gas supply and transport sector. Moreover, the combination of electricity and gas infrastructures may play an important role in the design of future RES systems, and the electrification of heating and transport can play a pivotal role in providing flexibility and ensuring RES integration in all sectors [23].

In order to stimulate automation of data processing and overall digitalization in energy, the EC has proclaimed a support to the development of all kind of the smart energy systems, where simultaneous use of the natural gas and RG will play one of the major sustainability ensuring roles. First, it will help achieve designated energy efficiency goals and, second, it will allow for cost-saving synergetic solutions at the early stages of the energy supply chain decarbonisation [24], [25].

Synergy of natural gas and RG, in particular, sustainable and green hydrogen, emphasises the need for a modern, smart and sustainable energy infrastructure to allow developing more flexible back-up and balancing power capacity, storage solutions and innovative demand-response mechanisms. In a nutshell, usage of green or sustainable hydrogen in smart energy systems would emerge as a concept of smart hydrogen, which combines the following options: a solution to the electrical grid network challenges faced by the mature RES electricity technologies, opportunities in hydrogen supply pathway, prospects for new hydrogen applications, creation of different and new trends in energy markets with power to X (hereinafter – P2X) technologies. The aim of smart hydrogen would be to create a hydrogen value chain that is optimal in technical performance and financial revenues. With this in mind, the concept of P2X refers to energy conversion technologies that allow for the decoupling of power production plants from the electrical market to use their product in a number of other sectors, such as transport, heating and chemical industry.

There is a belief that green and sustainable hydrogen network development should start at the energy transmission level, where the EU Hydrogen Backbone will be created by 2050 the latest [26], [27], and only then come down to reach distribution systems. This is a reason why transmission level projects and initiatives are more widespread and accounted for at the moment. Still at the distribution level, there are a few activities to address. For instance, in December 2021, DNV announced that it would lead a study aimed at the production of a roadmap for the European gas distribution networks to show how they could help unlock the growth potential of hydrogen distribution for wider and more feasible further use. The aim of the project is to combine the hydrogen expertise and experiences from across eighty European gas distribution companies and organisations [28]. It is planned that analysis of the European gas distributors will be performed in order to determine how they can contribute to the hydrogen development before drawing up a roadmap to show how gas distribution companies can support the transformation of Europe's primary hydrogen distribution infrastructure and enhance emerging smart energy systems in gas distribution. The European

gas distribution network consists of about 2 million kilometres of pipeline across the continent. It would be a significant benefit if large parts of the gas distribution network could be repurposed and extended, since they will drive the transition from natural gas to hydrogen at a lower cost compared to developing a new network [29].

For decades European local gas networks have shown the ability to deliver reliable, cost-effective and safe distribution to millions of customers, and it is strongly believed that local gas networks will also add value to address the challenges to achieve the huge growth and CO_2 reduction potential of hydrogen in Europe, as infrastructure provides the means to cope with rapidly growing shares of variable wind and solar power by transporting hydrogen from decentralized productions points to consumers throughout the EU market. The gas infrastructure has the capacity to handle demand seasonality providing reliable supply of hydrogen even during all periods of the year. Moreover, in this context large-scale hydrogen underground storage facilities linked to gas networks are considered to be the only fast-acting, long-lasting storage capacity at enormous scale to cope with variable power production and demand [12].

Also, local gas networks provide a flexible decarbonisation pathway for customers as they are well-positioned to distribute and manage varying local blends of molecules and, to a large extent, are ready to convert relatively quickly to pure hydrogen. Local gas network would facilitate a competitive and expanding hydrogen market, meaning more hydrogen for users at a lower price. At the same time, local gas networks provide a cost-efficient pathway, including significant volumes of hydrogen and biomethane, investment in the combined power and gas infrastructure [30]. Such initiatives are tended to contribute to significant financial savings, which are estimated to reach over 40 billion EUR a year.

To ensure a hydrogen pathway to smart gas distribution and, thus, a smart energy framework, hydrogen ready smart meters with capacity to extraordinary precision and versatility must be developed and tested in the prospect of wide hydrogen blending into the gas distribution networks in the EU. One option is to replace mechanical diaphragm meters with ultrasonic devices, which rely on accurate measurement of the speed of sound to determine the gas flow rate. Because the speed of sound in hydrogen is around three times faster than that in natural gas, significantly better timing precision is needed [31].

Also, the introduction of sustainable and green hydrogen as a replacement for natural gas, which is firmly on agenda, is set to require large-scale modification and probable eventual replacement of the gas distribution infrastructure and gas-powered appliances and other equipment. While there are supporters for pure hydrogen consumption, in practice in most cases its introduction is most likely to be blended with natural gas in proportions up to about 20 %, as the production and supply of green hydrogen is ramped up and the full hydrogen infrastructure is put in place [32].

Hydrogen energy content is about only one-third of natural gas. Thus, not only more hydrogen-blended natural gas is needed to deliver the same amount of energy to users compared to pure natural gas but also a higher volumetric flow rate is required. Options for the latter include increasing the operating pressure in the distribution system or replacing the existing pipelines with ones of larger diameter.

In case of its use in appliances, for example, the main concerns are potentially higher combustion temperatures with

hydrogen-natural gas blends, which could lead to local overheating of components, and the increase in the burning velocity, which poses a risk of potential flashbacks. Coupled with the changes on both the utility and consumer sides, there also will be a need for the changes in the primary interface, the meter, with eventual full gas smart meter replacement with hydrogen-ready or hydrogen only meters. At the moment, ultrasonic hydrogen meters are being developed, demonstrated and tested by several manufacturers, such as Pietro Fiorentini [33] and MeterTech [34]. It is expected that in close future these meters will be available on the market and ready for installation not only for large consumers, but also for households.

3. HYDROGEN AS AN ENABLER OF SECTORAL INTEGRATION

The versatility of hydrogen allows for wide potential energy sector integration as part of smart energy framework and, thus, contributes to the Europe's energy transition.

Power generation offers many opportunities for hydrogen and hydrogen-based fuels. In the near-term ammonia could be co-fired in coal-fired power plants to reduce CO_2 emissions. Hydrogen and ammonia can be flexible generation options when used in gas turbines or fuel cells. At the low-capacity factors typical of flexible power plants, hydrogen costing under USD 2.5/kg has good potential to compete. Key low-carbon competitors for such services include natural gas with CCS and biomethane. In the longer term, hydrogen can play a role in large-scale and long-term storage to balance seasonal variations.

It is believed that green and sustainable hydrogen, first and foremost, is meant to be used in decarbonisation of industry and energy generation processes, with smaller segments of energy sector not being the first priority. District and local heating are one of these sectors, where there is a great dispute on the necessity to include hydrogen in energy mix in Europe in a short- and mid-term perspective. According to the IEA, globally, district heating supplies a relatively small share of heat used in buildings, at only 8.5 % of the sector's heat consumption – a share that has remained impressively constant since 2000, considering that floor area has increased by 65 % at the same time. Although the global average share is low, district heating does cover a high portion of heat delivered to buildings in some European countries, such as Denmark and Sweden (both above 45 %) [35].

As usage of natural gas in district heating is still rather widespread in the EU and the United Kingdom, the injecting of up to 10 % hydrogen by volume into the natural gas transportation and distribution networks would not require any major alterations to equipment and would significantly reduce CO_2 [36] for households and small business consumers. At the same time, injection of up to 10 % hydrogen into the natural gas networks would contribute not only to district heating companies and their clients, but also to local and individual heating system users. They would also use hydrogen – natural gas – biomethane blend in their natural gas boilers and other equipment, not replacing them by new ones, and, at the same time, contributing to national and the EU emission reduction targets [37].

In the electricity sector, burning of liquid and gaseous hydrocarbons currently represents the largest share of electricity generation around the world. Countries with

limited RES and hydrocarbon resources rely significantly on expensive imported and polluting fuels. Importing electricity through transmission lines might sometimes be problematic due to high costs, system losses, and geographical barriers [37]. However, green hydrogen offers a viable alternative. Countries importing large amounts of hydrocarbons today, in the near future could switch to import of low-cost green hydrogen and convert it into electricity through large-scale fuel cells in domestic power plants [38]. Hydrogen concentrations of up to 10 % and 20 % are still permissible for the operation of turbines and compression stations, respectively, while pipelines can stand mixtures of up to 50 % (given some technical adjustments); anything above those values is currently still being researched [39]. For instance, Mitsubishi Hitachi Power Systems, Ltd. has recently disclosed the successful test of a large-scale highly efficient turbine fed with a 30 % hydrogen blend, attaining a stable combustion with a 10 % reduction in CO_2 emissions [40].

At the same time, hydrogen blending into the existing natural gas network has multiple advantages and can be a cost-effective transitional option in the short term in regions without parallel or duplicated networks. The retrofitting and repurposing of existing natural gas networks can be combined and complemented with the construction of new dedicated hydrogen infrastructure. It needs to be reminded that a purely hydrogen pipeline infrastructure is not a novelty. Such networks, although strictly compact and localized, are already used to supply single consumers, for example, petrochemical and fertilizer plant. At present, a 900 km long hydrogen pipeline network is built along the Gulf coast of the United States, which is regarded as the longest high-pressure hydrogen transportation network in the world [41]. In Europe, currently the largest and longest industrial hydrogen pipeline network is located in the area of ports of Rotterdam and Antwerp, with total length around 1500 km, where the longest part consists of small diameter distribution infrastructure [42]. In line with this, there are various initiatives, EHB and the Re-Stream studies carried out [43], in order to assess the potential of the existing European oil and gas infrastructure to carry hydrogen and/or carbon monoxide.

In addition, in the EU, a well-developed and regulated network of natural gas is already in place, with the transmission grid being approximately 2 million kilometres long.

A distribution grid, which is double the size of the current transmission grid, implies that the natural gas infrastructure is the key enabler for the deployment of a hydrogen economy. The UNECE Group of Experts on Gas recognised the key role of the natural gas transmission and distribution operators (*hereinafter* – TSO, DSO), natural gas industry and the natural gas infrastructure in the transition to a hydrogen economy through the energy system integration [44]. Even though pipelines and the natural gas storage facilities today are being considered the most cost-competitive solution for hydrogen distribution, numerous challenges remain. One of them is an increasing difficulty of building new pipelines, as many landowners are not ready to have such objects close to their properties. Thus, it is in the best interest of actors in the hydrogen value chain to find ways to extensively reuse existing natural gas infrastructure instead of constructing an entirely new hydrogen infrastructure. It is necessary to start immediate retrofitting and repurposing of current natural gas infrastructure. Given TSO and DSO know-how in operating natural gas transmission and distribution infrastructure, the gas TSOs should be among those certified as owners and operators of future hydrogen networks [45].

Authorizing the natural gas TSOs to carry out activities related to the development, integration and operation of hydrogen infrastructure would facilitate an efficient way forward due to their experience in planning, financing, constructing, operating and maintaining gas infrastructure, since existing gas grids will be retrofitted and repurposed for hydrogen [42].

One of the solutions to transform the gas network pipes suitable for hydrogen transportation is to use an inner coating. The inner coating would chemically protect the steel layer and reduce the hydrogen diffusion into the metal. This aspect might allow increasing the overall pressure in the tubes. Initial hydrogen conversion projects in Germany and the Netherlands have shown that existing pipelines in those regions do not require internal coating; studies in France show that re-coating can be a viable part of the optimisation solution by enabling pipes to be operated at pressures closer to the pressure of natural gas [46].

4. THE SITUATION OF LATVIA

In case of Latvia, hydrogen production targets are not included in the NECP, so the development of the sector is therefore not politically or legally governed by provisions of this document. Latvia also lacks a hydrogen strategy, which could be a substitute for it. In regard to hydrogen energy future plans, different estimates are made, studies performed and technical projects proposed. For instance, the study by "Fuel Cells and Hydrogen 2 Joint Undertaking" outlines the amount of green hydrogen used in the industry, transport and energy production, as planned for 2030. The study offers two scenarios for hydrogen demand: low and high. In a low hydrogen demand scenario, green hydrogen would account for 0.1 % of total final energy demand (0.05 terawatt-hours (*hereinafter* – TWh)), but in the high one – 0.5 % of the total final energy demand (0.2 TWh) [47].

Several hydrogen production and usage proposals can be mentioned among those, which can be implemented in foreseeable future. The plan for a hydrogen filling station near Ainazi wind park envisages that a green hydrogen production point and a filling station with 100 kilo-watt (*hereinafter* – kW) electrolyser would be built near Ainazu wind park [48].

With regard to smart energy systems and frameworks, larger initiatives are crucial. Projects conceived by Ventspils nafta terminals (*hereinafter* – VNT) and JSC Latvenergo should be pointed out. VNT intends to create a green hydrogen valley, which would provide not only hydrogen production and consumption, but locally integrated green hydrogen ecosystem for climate change mitigation and regional economic development. Hydrogen valley would cover a substantial part of the hydrogen value chain: production, storage, transportation, and various consumption options.

The hydrogen production project by JSC Latvenergo states that green hydrogen would be produced using a polymer electrolyte membrane electrolyser, and electricity needed for the process would come from the Daugava hydropower plants, Riga CHP-2 or from the planned new large-scale wind parks. The produced hydrogen would be stored or used immediately for combustion in gas turbines at CHP-2. Beforehand, the produced hydrogen would be blended with natural gas, so percentage of hydrogen in the gas mixture would not exceed 5 % by volume in order not to affect the opera-

tion of the plant equipment. Hydrogen storage is intended for its later use in cooling of the CHP-2 electric generators or for sale to local consumers such as transport companies or the industry [48]. Based on the initial research results, the electrolysis capacity of 6.5 MW was determined [49]. In-depth and detailed studies on the subject are currently underway with the involvement of external experts.

Another potential solution for the utilization of produced hydrogen is to inject it into the natural gas grid. JSC Latvenergo is also evaluating the possibilities to build a new interconnection to the gas transmission system. The potential transmission natural gas pipeline together with the existing distribution gas pipeline can be used to inject a mixture of hydrogen and methane into the gas grid. The hydrogen pilot project is planned to be implemented until 2025, but until 2030–2035 a larger capacity electrolysis plant (over 100 MW) would come online. For the production of green hydrogen, JSC Latvenergo plans to significantly increase the capacity of wind and solar plants as well, which can exceed 2000 MW in total installed capacity. Together with existing hydropower capacities, it can provide electrolysis plants with green electricity at competitive prices. In addition, production of green hydrogen in the small-scale hydropower plants has also been considered in scientific research [50].

5. CONCLUSIONS

Most likely, green and sustainable hydrogen will play an important role in the emerging European smart energy framework, as it opens many possible avenues for energy production, transportation and storage, while new technological and sectoral synergy options are explored further in order to make them the part of all the European energy supply chain, and not only a fraction of it.

Green and sustainable hydrogen provides an opportunity to extend the boundaries of smart energy system concept beyond the electricity sector, as hydrogen helps tackle both problems faced by the gas industry and electricity sector alike. It is not limited to one of these important segments of energy, and technical readiness of the infrastructure – primarily, of gas transmission and distribution, will be a critical link between the two.

The most effective and least-costly solutions in smart energy framework can be found, when the electricity sector is combined with the heating and cooling sectors, gas supply and transport sector. Moreover, the combination of electricity and gas infrastructures may play an important role in the design of future RES systems, and the electrification of heating and transport can play a pivotal role in providing flexibility and ensuring RES integration in all sectors.

Power generation also offers many opportunities for hydrogen and hydrogen-based fuels, as in the near-term ammonia could be co-fired in coal-fired power plants, but the hydrogen itself in gas-fired power plants to reduce CO_2 emissions. At the same time, hydrogen blending into the existing natural gas network has multiple advantages and can be a cost-effective transitional option in the short term in regions without parallel or duplicated networks. The retrofitting and repurposing of existing natural gas networks can be combined and complemented with the construction of new dedicated hydrogen infrastructure.

If even in Latvia hydrogen-based

energy initiatives of different scale are still a novelty, and the lack of definite hydrogen energy development strategic framework is obvious, there are several proposals to develop the hydrogen production and consumption value chain (or elements of it) both in isolated applications, like fuelling stations, and wider applications, like hydrogen valley envisaged by VNT. Industrial applications of hydrogen production and co-firing in gas power plants are also underway, as there is the theoretical possibility to feed the hydrogen into the gas transmission system.

ACKNOWLEDGEMENTS

The research has been supported by the National Research Programme, project "Trends, Challenges and Solutions of Latvian Gas Infrastructure Development" (LAGAS) (No. VPP-EM-INFRA-2018/1-0003).

REFERENCES

1. UN. (2020). *Long-Term Low Greenhouse Gas Emission Development Strategy of the European Union and its Member States*. Available at https://unfccc.int/documents/210328
2. IEA. (2019). *The Future of Hydrogen*. Available at https://www.iea.org/reports/the-future-of-hydrogen
3. IEA. (2021). *Global Hydrogen Review 2021*. Available at https://www.iea.org/reports/global-hydrogen-review-2021/executive-summary
4. Jansons, L., Bode, I., Zemite, L., Zeltins, N., Geipele, I., & Kiesners, K. (2022). Securing Sustainable Energy Future: Green Hydrogen as a Part of Gaseous Fuel Diversification Risk Management Strategy. *Latvian Journal of Physics and Technical Sciences*, 59 (4), 53–70. DOI: 10.2478/lpts-2022-0033
5. IEA. (2022). *Electrolysers. Technology Deep Dive*. Available at https://www.iea.org/reports/electrolysers
6. Power Technology. (2022). *Global Electrolyzer Capacity to Reach 8.52GW by 2026*. Available at https://www.power-technology.com/comment/global-electrolyzer-capacity/
7. Energy Transitions Commission. (2021). *Making the Hydrogen Economy Possible: Accelerating Clean Hydrogen in an Electrified Economy*. Available at https://www.energy-transitions.org/wp-content/uploads/2021/04/ETC-Global-Hydrogen-Report.pdf
8. Statista. (2021). *Number of Hydrogen Projects Announced Worldwide as of 2021, by Region*. Available at https://www.statista.com/statistics/1220805/global-hydrogen-projects-by-region/
9. Nnabuife, S.G., Ugbeh-Johnson, J., Evaristus Okeke, N., & Ogbonnaya, C. (2022). Present and Projected Developments in Hydrogen Production: A Technological Review. *Carbon Capture Science & Technology*, *3*. https://doi.org/10.1016/j.ccst.2022.100042
10. PWC. (n.d.). *The Green Hydrogen Economy. Predicting the Decarbonisation Agenda of Tomorrow*. Available at https://www.pwc.com/gx/en/industries/energy-utilities-resources/future-energy/green-hydrogen-cost.html
11. Jansons, L., Zeltins, N., Geipele, I., & Zemite, L. (2022). Gaseous Fuel Diversification in Residential Sector: Analysis of Potential Risks. *Scientific Problems of Engineering Economics of Construction and Real Estate Management, Regional and Territorial Development* (Section in the Annual 63rd International Scientific Conference of Riga Technical University), 29–30 September 2022. ISSN: 2592-9372.

12. Jansons, L., Geipele, I., Zemite, L., & Zeltins, N. (2022). Large-Scale Hydrogen Underground Storages and Associated Risk Factors. *Scientific Problems of Engineering Economics of Construction and Real Estate Management, Regional and Territorial Development* (Section in the Annual 63rd International Scientific Conference of Riga Technical University), 29–30 September 2022. ISSN: 2592-9372
13. EC. (2020). *Communication from the Commission to the European Parliament, the Council, the European Economic and Social Committee and the Committee of the Regions. A Hydrogen Strategy for a Climate-Neutral Europe*. Available at https://eur-lex.europa.eu/legal-content/EN/TXT/?uri=CELEX:52020DC0301
14. EC. (n.d.). *National Energy and Climate Plans. EU Countries' 10-Year National Energy and Climate Plans for 2021–2030*. Available at https://ec.europa.eu/info/energy-climate-change-environment/implementation-eu-countries/energy-and-climate-governance-and-reporting/national-energy-and-climate-plans_en#final-necps
15. IEA. (2022). *Hydrogen. Energy System Overview*. Available at https://www.iea.org/reports/hydrogen
16. HydrogenEurope.(2020).*Strategy:Hydrogen Europe's Top 10 Key Recommendations*. Available at https://hydrogeneurope.eu/wp-content/uploads/2021/11/The-EU-Hydrogen-Strategy_-Hydrogen-Europes-top-10-key-recommendations_FINAL.pdf
17. Vlaanderen. (n.d.). *Fuel Cells and Hydrogen 2 Joint Undertaking – (other organisations)*. Available at https://eufundingoverview.be/funding/fuel-cells-and-hydrogen-2-joint-undertaking-other-organisations
18. USEF. (2016). *An Introduction to the Universal Smart Energy Framework*. Available at https://www.usef.energy/app/uploads/2016/12/An-introduction-to-the-Universal-Smart-Energy-Framework-2.pdf
19. Mathiesen, B.V., Lund, H., Connolly, D., Østergaard, P. A., & Mölle, B. (2015). *The Design of Smart Energy Systems for 100% Renewable Energy and Transport Solutions*. DOI: 10.1016/j.apenergy.2015.01.075.
20. Savickis, J., Zemite, L., Jansons, L., Bode, I., Dzelzitis, E., Broks, A., & Vempere, L. (2020). The Development of the Smart Gas Distribution: General Trends and the Latvian Context. *Latvian Journal of Physics and Technical Sciences*, 57 (6), 23–39. DOI: 10.2478/lpts-2020-0031
21. Skov, I.R. (2015). *Integrated Electrofuels and Renewable Energy Systems*. PhD Thesis. Aalborg University. DOI: 10.13140/RG.2.1.4318.5682.
22. Fehrenbacher, K. (2009). *Why the Smart Grid Won't Have the Innovations of the Internet Any Time Soon*. Available at https://archive.nytimes.com/www.nytimes.com/external/gigaom/2009/06/05/05gigaom-why-the-smart-grid-wont-have-the-innovations-of-t-92813.html
23. Savickis, J., Zeltiņš, N., & Jansons, L. (2019). Synergy Between the Natural Gas and RES in Enhancement of Security of Energy Supply in the Baltic Countries (Problem Statement). *Latvian Journal of Physics and Technical Sciences*, 56 (6), 17–31. DOI: 10.2478/lpts-2019-0032
24. Savickis, J., Zemite, L., Zeltins, N., Bode, I., Jansons, L., Dzelzitis, E., … & Ansone, A. (2020). The Biomethane Injection into the Natural Gas Networks: The EU's Gas Synergy Path. *Latvian Journal of Physics and Technical Sciences*, 57 (4), 34–50. DOI: 10.2478/lpts-2020-0020
25. Kurmayer, N.J. (2023). *Germany to Almost Double Gas Firing Capacity*. Available at https://www.euractiv.com/section/energy/news/germany-to-almost-double-gas-firing-capacity/
26. ACER. (n.d.). *Gas Factsheet*. Available at https://www.acer.europa.eu/gas-factsheet
27. Wang, A., van der Leun, K., Peters, D., & Buseman, M. (2020). *European Hydrogen Backbone. How a Dedicated Hydrogen Infrastructure Can Be Created*. Available at https://gasforclimate2050.eu/wp-content/uploads/2020/07/2020_European-Hydrogen-Backbone_Report.pdf
28. Pekic, S. (2021). DNV Studies Hydrogen to Support Ready4H2 Roadmap. Available at https://www.offshore-energy.biz/dnv-studies-hydrogen-to-support-ready4h2-roadmap/

29. EHB. (n.d.). *The European Hydrogen Backbone (EHB) Initiative*. Available at https://ehb.eu/
30. Zemite, L., Bode, I., Vempere, L., Jasevics, A., Jansons, L., & Kleperis, J. (2022). Biogas Production Support Systems for the Production and Use of Biomethane. *Proceeding of the 22nd International Conference on Environmental and Electrical Engineering (EEEIC2022)*, 21 December 2021. DOI: 10.1109/EEEIC/ICPSEurope54979.2022.98547
31. Amicucci, L. (2020). *Cellular IoT Smart Meter Boosts Hydrogen Energy Sector*. Available at https://blog.nordicsemi.com/getconnected/cellular-iot-smart-meter-boosts-hydrogen-energy-sector
32. Jansons, L., Bode, I., Zemite, L., Zeltins, N., Geipele, I., Kiesners, K. (2022). Securing Sustainable Energy Future: Green Hydrogen as a Part of Gaseous Fuel Diversification Risk Management Strategy. *Latvian Journal of Physics and Technical Sciences*, 59 (4), 53–70. DOI: 10.2478/lpts-2022-0033
33. Fiorentini, P. (n.d.). *Residental Metering. H2 SSM*. Available at https://static1.squarespace.com/static/5b8eae345cfd799896a803f4/t/6231afa5a4627b0ff7abb563/1647423398301/h2ssm_flyer_ENG_revA.pdf
34. MeterTech. (n.d.). *What we do. Bespoke Solutions for your Metering Needs*. Available at https://metertech.co.uk/what-we-do
35. Jaribion, A., Khajavi, S., Ohman, M., Knapen, A., & Holmstrom, J. (2020). A digital twin for safety and risk management: A prototype for a hydrogen high-pressure vessel. In *15th International Conference on Design Science Research in Information Systems and Technology*, (pp. 369–375), 2–4 December 2020. Kristiansand, Norway. doi: 10.1007/978-3-030-64823-7_34
36. Savickis, J., Zemite, L., Jansons, L., Bode, I., Dzelzitis, E., Broks, A., Vempere, L. (2020). The Development of the Smart Gas Distribution: General Trends and the Latvian Context. *Latvian Journal of Physics and Technical Sciences*, 57 (6), 23–39. DOI: 10.2478/lpts-2020-0031
37. ADBA. (2021). *Biomethane & Hydrogen. Two Green Gases, One Future. Biogas Insights*. Available at https://www.greengastrading.co.uk/wp-content/uploads/2021/07/ADBA-Hydrogen-and-biomethane-Decarbonising-gas.pdf
38. PwC. (2020). *The Dawn of Green Hydrogen. Maintaining the GCC's Edge in a Decarbonized World*. Available at https://www.strategyand.pwc.com/m1/en/reports/2020/the-dawn-of-green-hydrogen/the-dawn-of-green-hydrogen.pdf
39. Bolobov, V.I., Latipov, I.U., Popov, G.G., Buslaev, G.V., & Martynenko, Y.V. (2021). Estimation of the Influence of Compressed Hydrogen on the Mechanical Properties of Pipeline Steels. *Energies*, 14.
40. Mitsubishi Power. (n.d.). *MHPS Successfully Tests Large-Scale High-Efficiency Gas Turbine Fuelled by 30 % Hydrogen Mix*. Available at https://power.mhi.com/news/20180119.html
41. Air Products. (2012). *Air Products' U.S. Gulf Coast Hydrogen Network Enhanced Reliability from the World's Largest Hydrogen Pipeline*. Available at https://microsites.airproducts.com/h2-pipeline/pdf/air-products-us-gulf-coast-hydrogen-network-datasheet.pdf
42. UNECE. (2021). *Technology Brief. Hydrogen*. Available at https://unece.org/sites/default/files/2021-10/Hydrogen%20brief_EN_final_0.pdf
43. Re-Stream. (2021). *Study on the Reuse of Oil and Gas Infrastructure for Hydrogen and CCS in Europe*. Available at https://www.concawe.eu/wp-content/uploads/Re-stream-final-report_Oct2021.pdf
44. UNECE. (2020). *Report of the Group of Experts on Gas*. Available at https://unece.org/sed/documents/2022/04/reports/report-group-experts-gas
45. ENTSOG. (2021). *ENTSOG Summary of Proposals for Addressing Hydrogen Regulation in the Revision of the 3rd Energy Gas Package*. Available at https://www.entsog.eu/sites/default/files/2021-06/202106%20-%20Position%20-%20ENTSOG%20-%20Open%20PC%20Hydrogen%20Gas%20Market%20Decarbonisation%20Package.pdf

46. Kleperis, J., Boss, D., Mezulis, A., Zemite, L., Lesnicenoks, P., Knoks, A. & Dimanta, I. (2021). Analysis of the Role of the Latvian Natural Gas Network for the Use of Future Energy Systems: Hydrogen from RES. *Latvian Journal of Physics and Technical Sciences*, *58* (3), 214–226. doi: 10.2478/lpts-2021-0027
47. FCHO. (2020). Opportunities for Hydrogen Energy Technologies Considering the National Energy & Climate Plans. Available at https://www.fchobservatory.eu/news-events/new-study-released-opportunities-hydrogen-energy-technologies-considering-national
48. Stepiņa, K. (2022). *Arī Latvijā ir iespējas ražot ūdeņradi no atjaunojamajiem resursiem*. Available at https://www.retv.lv/raksts/ari-latvija-ir-iespejas-razot-udenradi-no-atjaunojamajiem-resursiem
49. Elektrum. (2022). *Elektroenerģijas tirgus apskats*. Available at https://latvenergo.lv/storage/app/media/uploaded-files/ETA_jan_2022.pdf
50. Zemite, L., Kobzars, V., & Jansons, L. (2022). Water Energy – for the Production of Hydrogen? Low Power HES and Their Perspective. *Enerģija un Pasaule, 1*, 34–39.

sciendo

LATVIAN JOURNAL OF PHYSICS
AND TECHNICAL SCIENCES
2023, N 1

DOI: 10.2478/lpts-2023-0004

ENERGY PERFORMANCE ASPECTS OF RESIDENTIAL BUILDINGS IN LATVIA

A. Kundziņa[1], I. Geipele[1]*, M. Auders[2], S. Lapuķe[1]

[1] Riga Technical University,
Institute of Civil Engineering and Real Estate Economics
6 Kalnciema Str., Riga, LV-1048, LATVIA
[2] Ministry of Economics of the Republic of Latvia,
Department of Housing Policy
55 Brīvības Str., Riga, LV-1519, LATVIA
*e-mail: Ineta.Geipele@rtu.lv

Measures on increasing energy efficiency is a way for ensuring sustainable energy supply, reducing emission of gases causing the greenhouse effect, improving safety of energy supply, decreasing dependence on import of energy and promoting the EU competitiveness. Improvement of energy performance of buildings as a direction of activities is provided in national policy planning documents of major importance such as the National Energy and Climate Plan for 2021–2030 and the Strategy of Latvia for the Achievement of Climate Neutrality by 2050.

Residential buildings form a considerable part of the total Latvian housing stock – 27 % according to the number of buildings and 44 % according to their area. Therefore, the increase of energy performance of residential buildings is very significant for achieving the national energy saving targets, i.e. a cumulative savings of final energy consumption of about 6 PJ by 2030.

The research analyses the sector of residential buildings, their statistical data, the energy consumption and requirements of the energy performance standards. To characterise this sector more comprehensively, information has been evaluated on energy performance certificates of residential buildings issued during the period from 2016 to 2021, allowing the authors to make general conclusions on the energy performance level of residential buildings and to provide proposals for increasing their energy efficiency.

Keywords: *Building energy performance class and index, energy efficiency, energy performance certificate, residential buildings.*

1. INTRODUCTION

Energy consumption and reduction of its inexpedient usage are the increasingly topical issues in the European Union (EU). Measures on increasing energy efficiency is a way for ensuring sustainable energy supply, reducing emission of gases causing the greenhouse effect, improving safety of energy supply, decreasing dependence on import of energy and promoting the EU competitiveness. In accordance with the EU Directive on the energy performance of buildings [1], by 2030, the EU needs to reduce energy consumption by at least 32.5 %, which is expressed as primary energy consumption and final energy consumption – in absolute figures, the reduction being correspondingly 1273 Mtoe and 956 Mtoe in 2030. Each EU Member State has developed its integrated national energy and climate plan (NECP) for 2021–2030 [2], declaring its intention to achieve the set energy saving targets by 2030. The Latvian mandatory national target in the building energy performance field for 2021–2030 is cumulative end-use energy savings of 1.76 Mtoe (73.72 PJ).

One of the directions of activities according to the Latvian National Energy and Climate Plan for 2021–2030 is improvement of energy performance of buildings. The measures for their improvement [3] should not only include renovation of the existing buildings, but also should ensure construction of new residential buildings [4] and their compliance with the energy performance requirements. To achieve the set energy savings, it is planned to reduce energy consumption in the household sector by 0.3 Mtoe (12.4 PJ), which is 17 % of the national target. About a half of the planned energy savings pertains directly to increasing energy performance of residential buildings and the other half involves a decrease of electric energy consumption for lighting and operation of different devices.

The Strategy of Latvia for the Achievement of Climate Neutrality by 2050 [5] stipulates that in order to achieve climate neutrality in Latvia by 2050, one of the main tasks is to increase energy efficiency in all sectors of national economy, including the housing sector, which has a significant potential for achieving the common energy efficiency targets.

2. CURRENT SITUATION AND PROBLEMS

In accordance with the Cabinet Regulation No 326 "Structure Classification Regulations" [6], structures are divided into buildings and engineering structures. Buildings are divided into residential and non-residential.

Main *groups* of residential buildings, in accordance with the aforementioned regulations, are as follows:

- one-dwelling buildings (code 111);
- two and multi-dwelling buildings (code 112);
- shared houses for different social groups (code 113).

When dividing further into *classes*, two- and multi-dwelling buildings are divided into two-dwelling buildings (code 1121) and three-and multi-dwelling buildings (code 1122). The classification of structures is schematically depicted in Fig. 1.

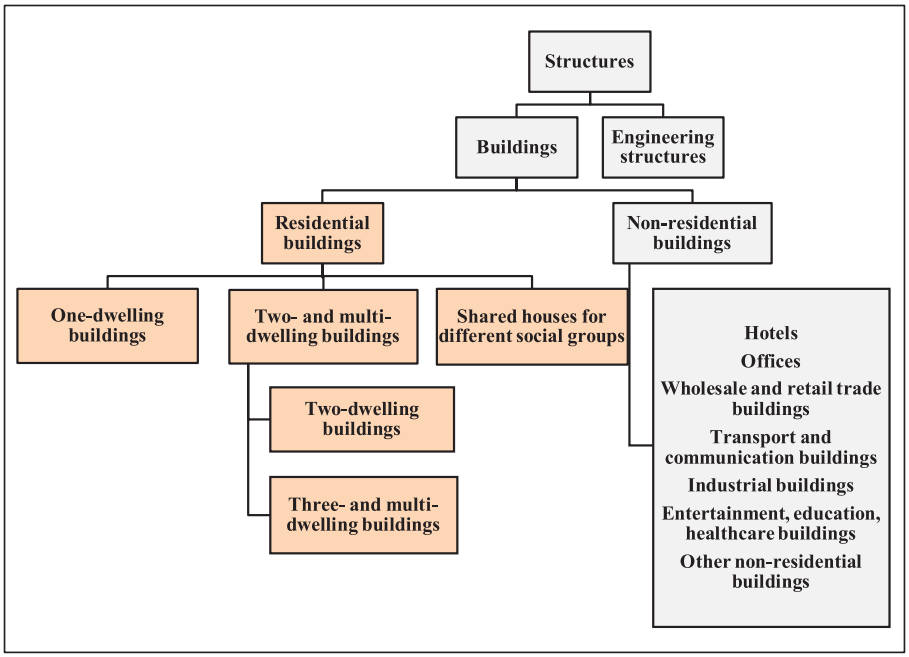

Fig. 1. Classification of structures [6].

In accordance with the State Land Service data [7], as of 1 January 2022, 1 373 642 buildings were registered in Latvia, of which 368 038 (26.8%) were residential and 1 005 604 (73.2%) non-residential. All buildings occupy the area of 206.6 mln.m^2; residential buildings occupy 91.1 mln.m^2 (44.1%) and non-residential 115.5 mln.m^2 (55.9%). Residential buildings form a considerable part of the total Latvian housing stock – 27 % according to the number of buildings and 44 % according to their area. The division of residential buildings by *classes*[1] according to their number and area is provided in Fig. 2.

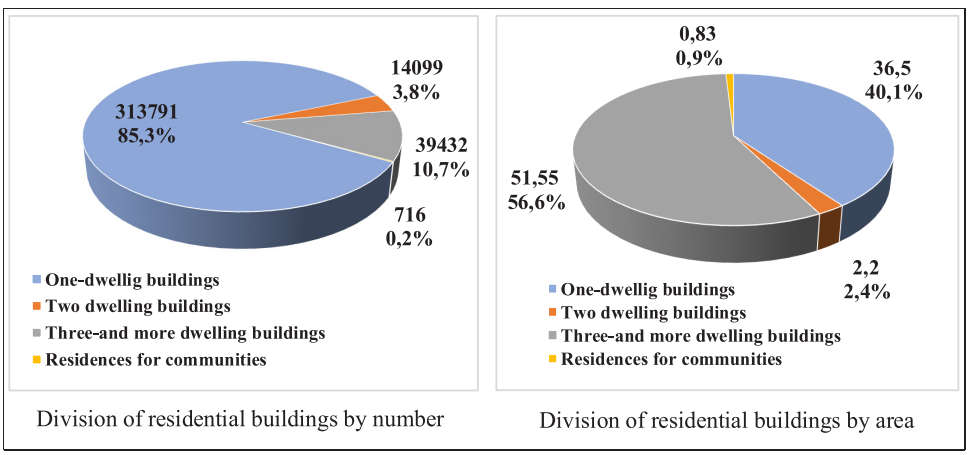

Fig. 2. Division of residential buildings by number and area [7], [8].

[1] Information in the statistical data of the State Land Service is provided by classes of buildings

The bulk of residential buildings – 313.8 thousand or 85.3% – are one-dwelling buildings. The next biggest group are three- and multi-dwelling buildings (39.4 thousand or 10.7%), followed by two-dwelling buildings – 14.1 thousand or 3.8%. The number of shared houses for different social groups is not big – 716 or 0.2%.

When analysing the division by area, three- and multi-dwelling buildings occupy the biggest area (51.55 mln.m^2 or 56.6%), then follow one-dwelling buildings – about 36.5 mln.m^2 or 40.1%, two-dwelling buildings – about 2.2 mln.m^2 or 2.4%. Shared houses for different social groups occupy the area of 0.83 mln.m^2 or 0.8 %.

When looking at Latvian official statistical[2] data regarding new and reconstructed residential buildings [9], [10] during the period of 2010 to 2021 (Table 1), one can conclude that only 5.5 % new buildings were built and 3.2 % were reconstructed from the total area of residential buildings during this period. One-dwelling buildings dominate among new buildings (9.1 %) and shared houses for different social groups among reconstructed ones (20.4 %).

Table 1. New and Reconstructed Residential Buildings (2010–2021), thous. m^2 [9]

Building type	**All residential buildings**	**New residential buildings**		**Reconstructed residential buildings**	
One-dwelling buildings	36500	3320.7	9.1 %	1776.2	4.9 %
Two- and multi-dwelling buildings	53750	1648.1	3.1 %	983.8	1.8 %
Shared houses for different social groups	830	43.6	5.3 %	169.4	20.4 %
Total	**91080**	**5012.4**	**5.5 %**	**2929.4**	**3.2 %**

In accordance with the statistical data [11], during the period of 2008–2020, the final energy consumption of households fluctuated from 46.3 to 64.3 and, on average, constituted 53.3 PJ a year or 31 % of the total final consumption. The most stable was electric energy consumption, which during this period fluctuated within the borders from 5.9 to 7.3 PJ (6.5 PJ on average). The heat energy consumption (centralised heat supply) was within the borders from 14.1 to 17.6 PJ (15.5 PJ on average) and the consumption of fuel for heating – within the borders from 25.9 to 40.8 PJ (31.3 PJ on average). Figure 3 provides the dynamics of final energy consumption of households during the period of 2008–2020.

It has to be noted that the district heat supply services are mainly used by multi-dwelling buildings and heating fuel for obtaining heat energy in direct way is primarily consumed by one-dwelling buildings.

[2] The division *in groups* is used on the Latvian official statistics portal

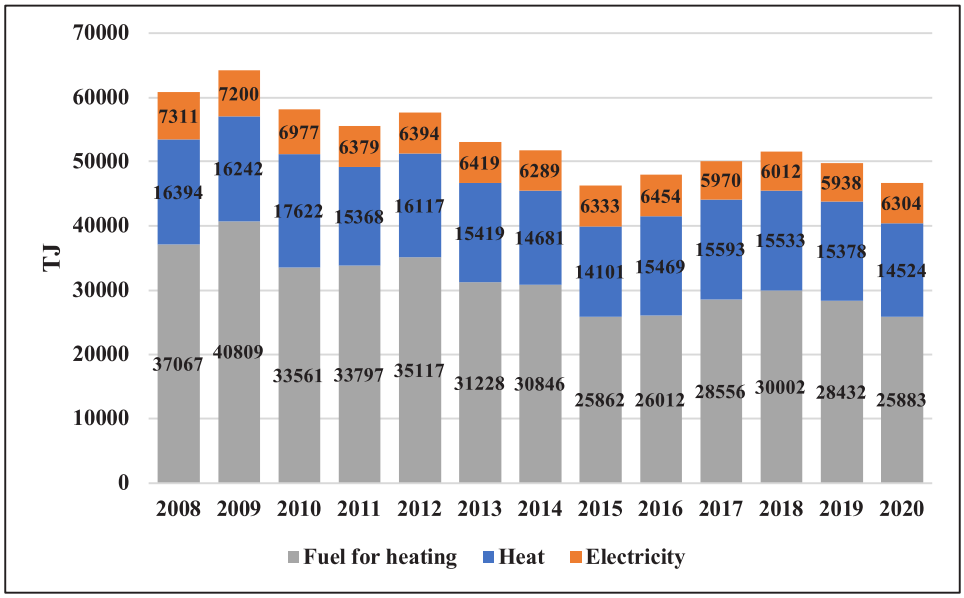

Fig. 3. Division of final energy consumption at households, TJ [11].

When analysing the dynamics of energy consumption, one can conclude that during the 12-year period the energy consumption has the characteristic tendency to reduction (see Fig. 4). The main reasons for the energy consumption changes are as follows:

- change of climatic conditions;
- changes in the number of consumers;
- changes in the areas of residential areas;
- effect of measures to increase energy efficiency;
- different economic and social factors – mostly income.

Thus, for example, during the surveyed period, the number of residents in Latvia [12] decreased by almost 300 thousand (12.9 %), and the housing stock increased [13] by almost 10 million m^2 or 14.5 %. The number of residents is directly related to the number of energy consumers; therefore, it enables reduction of electric energy and hot water consumption. Whereas, the growth of the housing stock area increases the amount of energy required for heating.

Latvian climatic conditions differ from year to year and depend also on the geographical location of the place of residence. Still, the general tendency for the average temperature during the heating period of the surveyed 12 years is to be growing [14], and, therefore, it can be assumed that the climatic conditions enable reduction of energy consumption for the needs of heating.

Similarly, reduction of energy consumption was promoted by measures to increase energy performance of buildings implemented during the last decade.

A significant impact on the energy consumption at households is also left by economic and social factors influencing the consumers – thus, for instance, an income level decrease can limit the consumption and decrease the comfort level and vice versa. Still, the income level factor cannot be evaluated unequivocally, as a high income can also promote reduction of energy consumption, when high-quality energy-efficient devices are acquired, as well as change of habits and formation of a conscientious attitude (choice of energy-

efficient devices and technologies, regulation of consumption, etc.) promote reduction of energy consumption.

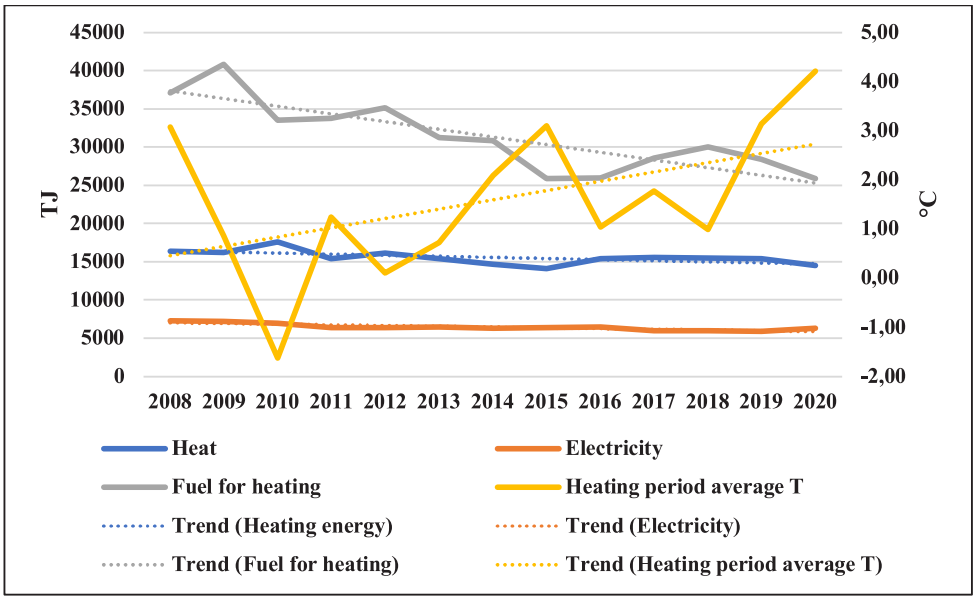

Fig. 4. Energy consumption dynamics and dependence on climatic conditions [11], [14].

The sector of residential buildings, on average, consumes 47 PJ a year for space heating and domestic hot water. For district heat supply, space heating constitutes 65–70 % and hot water supply 30–35 % [15]. For a local heat supply, this ratio could be similar; thus, it can be assumed that 70 % or 33 PJ of energy are consumed for the needs of heating.

In the context of energy performance of buildings, attention should be focused on residential buildings which are heated. One can assume that practically all two-, three- and multi-dwelling buildings are heated, as well as shared houses for different social groups. With regards to one-dwelling buildings, this group of buildings also includes summer houses and garden-houses, which are not heated at all or are not heated during a part of the heating season. The Long-term Strategy for Building Renovation stipulates that out of all one-dwelling buildings about 75 % are heated. It means that 236 thousand one-dwelling buildings are heated.

As of 1 January 2020, the Latvian Construction Standard LBN 002-19 "Thermotechnics of Building Envelopes" took effect, replacing the previous Construction Standard LBN 002-15. The new Construction Standard has stricter requirements to the minimum allowed level of energy performance of buildings, the energy performance assessment for heating renovation and reconstruction starting from 2021, in order:

- to fulfil the requirements of the Directive 2010/31/EU of the European Parliament and of the Council of 19 May 2010 on the energy performance of buildings, which stipulate that the State should promote renovation of buildings making them almost zero-energy buildings,
- to achieve the building decarbonisation target by 2050.

LBN 002-19 [16] prescribes that starting from 1 January 2021, the minimum allowed level of energy performance of new buildings is their conformity to the almost zero-energy building. In the event of building renovation or reconstruction, the minimum allowed level of energy performance at multi-dwelling buildings may not exceed 80 kWh/m^2 a year and 90 kWh/m^2 a year at one- or two-dwelling buildings.

The requirements of the almost zero-energy building are prescribed by the Cabinet Regulation No 222 "Building Energy Performance Calculation Methods and Building Energy Certification Regulations" [17], and the energy consumption of such building for heating may not exceed the provided level for the A Class building – 40, 50 or 60 kWh/m^2 a year, depending on the area of the building (Table 2). Similar requirements pertain also to the primary consumption of non-renewable energy of the building, which may not exceed the provided values for the A Class building. Energy consuming devices of engineering systems installed in the building must comply with the eco-design requirements and their energy marking – of at least A class. Moreover, compliance of the microclimate of premises with the construction regulatory enactments and the requirements in the field of hygiene and occupational safety must be ensured in the building.

Table 2. Minimum Allowed Heating Consumption Level of the Building Energy Performance, kWh/m^2 a year [17]

Building's energy performance class	Residential and non-residential buildings		Residential buildings
	Heated area, m^2		
	50-120	120-250	Over 250
			Residential houses
A	≤60	≤50	≤40
B	≤75	≤65	≤60
C	≤95	≤90	≤80
D	≤150	≤130	≤100
E	≤180	≤150	≤125
F	>180	>150	>125

To determine the minimum allowed heating consumption level, the "Building Energy Performance Calculation Methods and Building Energy Certification Regulations" take into account the area of heated premises of the building, which was not done before 2021. The heating consumption level of the building with the area of up to 250 m^2 is set higher than for buildings with the area exceeding 250 m^2, this way taking into account the ratio of the heated areas and the building envelopes.

3. DISCUSSION AND RESULTS

In accordance with the EU Directive [1] requirements, energy certification of buildings was started in Latvia in 2010 and was regulated by the Cabinet Regulation No 504 (8 June 2010) "Regulations on Energy Certification of Buildings". In 2013, this Regulation was replaced by the Regulation No 383 (9 July 2013) having the same title, and the Cabinet Regulation No 222 (8 April 2021) "Building Energy Efficiency Calculation Methods and Building Energy Certification Regulations" took effect in 2021.

Until 2016, energy certificates were issued in paper form, and there are no data available regarding how many and what type certificates were issued during that period. Since 2016, independent experts have been registering energy performance certificates of buildings in the Construction Information System (BIS) and they are publicly available.

In accordance with the Law on the Energy Performance of Buildings [18], energy certification is performed for the following residential buildings:

- for a building to be designed, rebuilt, or renewed in order to accept it for service or sell it;
- for an existing building in order to sell, rent, or lease it;
- in cases where a building owner has taken a decision on certification of the energy performance of the building.

This research uses the list of building energy performance certificates of the State Construction Control Bureau of Latvia (SCCB) published on the Latvian Open Data Portal [20] and the Construction Information System [19].

When analysing information available in the Register of Energy Performance Certificates, one can conclude that errors were admitted when entering data on the type of energy certificates – for instance, when searching for energy certificates[3] of 2021, a list appears, which includes also a big number of temporary energy performance certificates (especially regarding one- and two-dwelling buildings). Such errors can be revealed easily, when viewing the list of energy performance certificates and fixing their issue date and validity period. Whereas, the Open Data Portal has incompletely entered data for 2021, as the number of energy performance certificates in the BIS register is bigger. The publication on the statistics of building energy performance certificates [21] notes that documents with the expired validity were also erroneously added to the valid temporary energy performance certificates. The admitted errors encumber summarising and analysing the information, still the deficiencies mentioned in the research are taken account of and are eliminated when considering separate parts of the register manually.

As of the start of 2022, 1789 energy performance certificates of residential buildings were registered in the BIS energy performance certificate register. 95 % or 1698 of energy performance certificates of residential buildings were issued to multi-dwelling buildings and only 5 % (91) energy performance certificates to one- and two-dwelling buildings.

Based on the BIS data, energy performance of the energy certified multi-dwelling residential buildings has been analysed. The aggregate of the surveyed data forms a rather small part (4.3 %) of the total number of multi-dwelling buildings; still, it is big enough to characterise the situation with residential buildings in general and to make general conclusions. Energy performance of one- and two-dwelling buildings has not been evaluated separately in the research, as the number of the available energy performance certificates is too small.

As the type of building must be provided in the building's energy performance certificate in accordance with the LVS EN ISO 52000-1:2017/NA:2020 Standard "Energy Performance of Buildings. Overarching EPB Assessment. Part 1: General Framework and Procedures", Table 4 of the NA Annex, where new categories of buildings appear, they have been adjusted with

[3] The validity period of a building's energy performance certificate is 10 years and that of a temporary energy performance certificate is three years

the classification of buildings provided in the Cabinet Regulation No 326 "Structure Classification Regulations".

Residential buildings are divided in the Register of Energy Performance Certificates of the Construction Information System (BIS) as follows:

- one household houses of different types (codes 1110 – one-dwelling buildings and 1121 – two-dwelling buildings);
- multi-dwelling buildings (1122);
- shared houses for different social groups (1130);
- residential buildings for public use (tenement houses, houses with shared premises) (12110102);
- mobile houses (111001);
- weekend houses (111001).

Currently, residential buildings can be searched for in the BIS Register of Energy Performance Certificates following their division into "multi-dwelling building" and "one- or two-dwelling building of a different type".

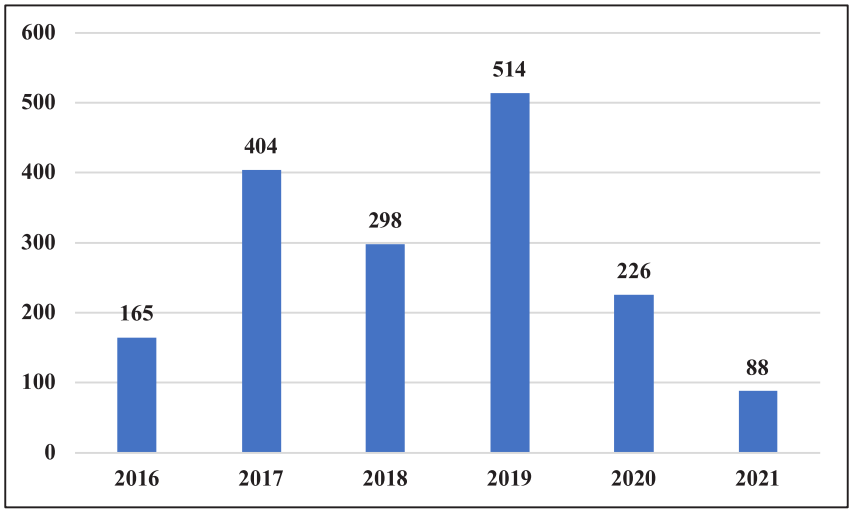

Fig. 5. Dynamics of registering energy performance certificates of multi-dwelling buildings [19].

When analysing the dynamics of issuing energy performance certificates for multi-dwelling buildings (Fig. 5), one can conclude that energy certification took place unevenly. To a large extent this dynamic is related to the EU funds co-financing programme [3], as an energy performance certificate is a compulsory requirement for submitting an application to receive co-financing from the EU funds. Within the framework of the 4th priority trend measure 4.2.1.1 "To promote increase of energy performance at residential buildings" of the EU funds for the 2014–2020 planning period, as of the start of 2022, there were 824 agreements [22] concluded to increase energy performance of multi-dwelling buildings. As the number of applicants was bigger, one can conclude that the bulk of energy performance certificates were required in order to enable participating in the selection for receiving co-financing from the EU funds.

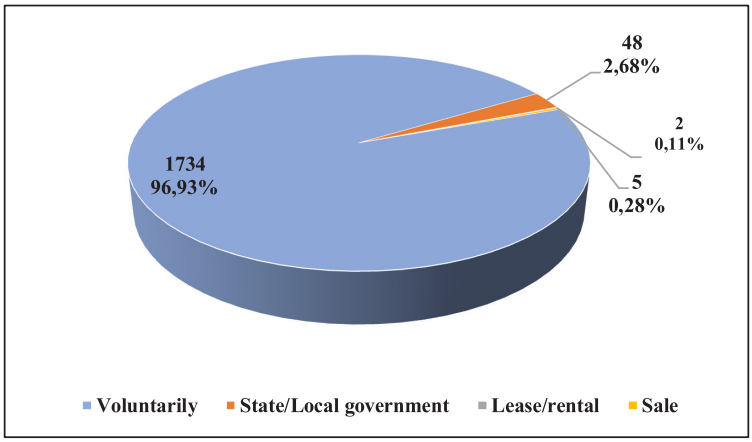

Fig. 6. Purposes of energy performance certification of residential buildings [20].

When analysing the purposes of issuing energy performance certificates for multi-dwelling buildings (Fig. 6), one can conclude that energy certification of almost all buildings (96.9 %) was performed voluntarily. In 48 cases (2.68 %), the building belonged to the State or a local government and its energy certification was mandatory. Only in some cases an energy performance certificate was required to sell or lease a building. This is explained by the fact that multi-dwelling buildings are predominantly divided into apartment properties, and an energy performance certificate is not required to sell or lease a separate apartment. Voluntary energy performance certification includes also cases, when co-financing from the EU funds is planned to be attracted for a building.

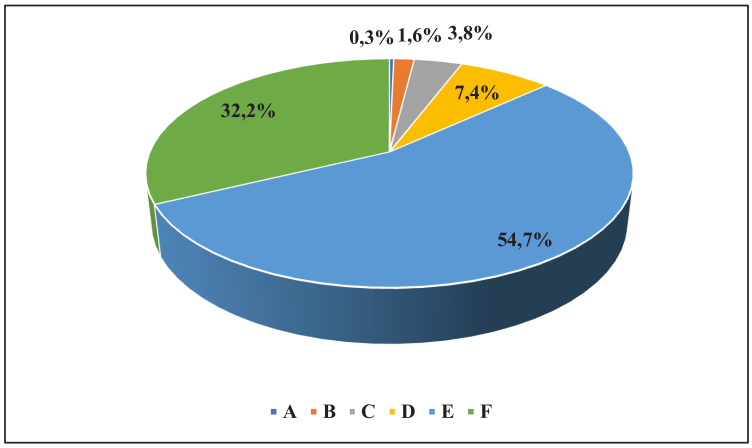

Fig. 7. Division of energy performance levels of residential buildings [19], [20].

Figure 7 demonstrates a summary on energy performance classes of residential buildings. The biggest proportion (54.7 %) is for the E class buildings, then follow the F class buildings – 32.2 %. 7.4 % of buildings correspond to the D class, 3.8 % to the C class, and only about 2 % of buildings to the A and B classes. In total, almost 90 % of energy certified residential buildings correspond to the lowest energy performance

classes. The average heating consumption level is 137 kWh/m^2 a year.

Herewith it has to be noted that the average energy performance level of Latvian multi-dwelling buildings is a little lower (in accordance with the SCCB information, in 2020 it was 125.6 kWh/m^2 a year), as the bulk of energy certified buildings were the ones where it was planned to attract the EU financing to perform measures for increasing the energy performance of the buildings. A grant for implementing measures to increase the energy performance was awarded [23], when the internal rate of return from the energy performance increase measures during the period of 35 years was bigger than 0. The method for calculating the size of the grant for implementing the project was based on the heating tariffs and the investment repayment period. As the average heating tariff during the period of 2016–2021, in comparison with the current situation, was low and stayed within the borders of 53 to 59 EUR/MWh [24], then energy efficiency measures of only such buildings could be cost-effective within 35 years, whose heat consumption level was high – corresponded to the F class.

4. CONCLUSIONS

One of the directions of activities according to the Latvian National Energy and Climate Plan for 2021–2030 is improvement of energy performance of buildings. The increase of energy performance of residential buildings is very significant for achieving the national energy saving targets, i.e. a cumulative savings of final energy consumption of about 6 PJ by 2030.

Residential buildings form a considerable part of the total Latvian housing stock – 27 % according to the number of buildings and 44 % according to their area. During the period of 2010 to 2021, only 5.5 % new buildings were built and 3.2 % were reconstructed from the total area of residential buildings.

During the period of 2008–2020, the final energy consumption (heat energy, electric energy and fuel for heating and hot water) of the household sector, on average, constituted 53.3 PJ a year or 31 % of the total final consumption. The heat energy consumption (district heating) was 15.5 PJ on average and the consumption of fuel for heating (individual heat supply) was 31.3 PJ on average. To ensure heating of residential buildings, on average, 33 PJ of energy were consumed a year.

When studying energy performance certificates of 1698 multi-dwelling buildings for the period of 2016–2021, one can conclude that the purpose of energy certification was predominantly voluntary energy certification (96.9 %), in 2.68 % of cases it was compulsory, as the building belonged to the State or a local government, and only in some cases (0.39 %) an energy performance certificate was required to sell, lease or take on lease the building.

Voluntary energy performance certification includes also cases, when co-financing from the EU funds is planned to be attracted for a building. With account of the fact that during the 2014–2020 EU funds planning period, as of the start of 2022, there were 824 agreements concluded to increase energy performance of multi-dwelling buildings, but the number of applicants was bigger, one can conclude that the bulk of energy performance certificates were required in order to enable participating in the selection for receiving co-financing from the EU funds.

The biggest proportion (54.7 %) is for the E class buildings, then follow the F class buildings – 32.2 %. 7.4 % of buildings correspond to the D class, 3.8 % to the C class, and only about 2 % of buildings to the A and B classes. In total, almost 90 % of energy certified residential buildings correspond to the lowest energy performance classes. The average heating consumption level is 137 kWh/m^2 a year.

Up to now, the support by using the EU funds, State and other support instruments has been provided to multi-dwelling buildings, but one-dwelling buildings (private houses) have been supported in a minimal volume. However, as in Latvia, on average, private houses are much less efficient than multi-dwelling buildings, it is required to provide support also to energy performance increase measures performed by private houses. Starting from April 2022, owners of private houses can apply for the support [25], which is anticipated in the form of grants, technical assistance and guarantees.

ACKNOWLEDGEMENT

This research was funded by the Latvian Science Council's fundamental and applied research programme project "Development of model for implementation of sustainable and environmentally friendly last-mile distribution transportation services in Latvia" (TRANS4ECO), project No. lzp-2022/1-0306, 01.01.2023.- 31.12.2025.

REFERENCES

1. Eur-Lex. (2020). *Directive 2010/31/EU of the European Parliament and of the Council of 19 May 2010 on the Energy Performance of Buildings.* Available at https://eur-lex.europa.eu/legal-content/EN/TXT/?uri=celex:32010L0031
2. Ministry of Economics. (2020). *National Energy and Climate Plan for 2021–2030.* Available at https://ec.europa.eu/energy/sites/ener/files/documents/lv_final_necp_main_en.pdf
3. Upitis, M., Amolina, I., Geipele, I., & Zeltins, N. (2020). Measures to Achieve the Energy Efficiency Improvement Targets in the Multiapartment Residential Sector. *Latvian Journal of Physics and Technical Sciences, 57* (6), 40–52. doi:10.2478/lpts-2020-0032
4. Tupenaite, L., Kaklauskas, A., Lillc, I., Geipele, I., Naimavičiene, J., Kanapeckiene, L., & Kauskale, L. (2018). Sustainability Assessment of the New Residential Projects in the Baltic States: A Multiple Criteria Approach. *Sustainability, 10* (5). 1387, https://doi.org/10.3390/su10051387
5. Ministry of Environmental Protection and Regional Development of the Republic of Latvia. (2020). *Informative Report "Strategy of Latvia for the Achievement of Climate Neutrality by 2050*". Available at https://unfccc.int/sites/default/files/resource/LTS1_Latvia.pdf
6. Cabinet Regulation No 326. (2018). *Structure Classification Regulations.* Available at https://likumi.lv/ta/id/299645-buvju-klasifikacijas-noteikumi
7. State Land Service (2021). *Reģistrēto būvju skaits sadalījumā pa galvenajiem lietošanas veidiem.* Available at https://www.vzd.gov.lv/lv/registreto-buvju-skaits-sadalijuma-pa-galvenajiem-lietosanas-veidiem
8. Ministry of Economics. (2020). *Informative Report "Long-term Strategy for Building Renovation".* Available at https://energy.ec.europa.eu/system/files/2021-01/lv_2020_ltrs_official_translation_en_0.pdf
9. Official Statistical Portal. (2022). *Commissioned Buildings by Building Type, Region and City.* Available at https://data.stat.gov.lv/pxweb/en/OSP_PUB/START/BUE030

10. Dimdina, I., Lešinskis, A. Krumiņš, E., Krumiņš, V., Snidere, L., & Zagorskis, V. (2011). Indoor air quality and energy efficiency in multi-apartment buildings before and after renovation: A case study of two buildings in Riga. In: *Civil Engineering '11: 3rd International Scientific Conference: Proceedings* (pp. 236–241), 12–13 May 2011. Jelgava: Latvia University of Agriculture, Latvia. ISSN 2255-7776.
11. Official Statistical Portal. (2022). *Energy Balance.* Available at https://data.stat.gov.lv/pxweb/en/OSP_PUB/START__NOZ__EN__ENB/ENB060
12. Official Statistical Portal. (2022). *Population at the Beginning of Year*. Available at https://data.stat.gov.lv/pxweb/en/OSP_PUB/START__POP__IR__IRS/IRS010/
13. Official Statistical Portal. (2021). *Housing Stock in Regions at the End of Year 2010–2020*. Available at https://data.stat.gov.lv/pxweb/en/OSP_PUB/START__NOZ__BU__BUF/BUF010
14. Official Statistical Portal. (2022). *Mean Monthly Air Temperature in Latvia*. Available at https://data.stat.gov.lv/pxweb/en/OSP_OD/OSP_OD__vide_geogr__geogr/GZG070.px/
15. RTU Institute of Environmental Protection and Heating Systems (2018). *Latvijas siltumapgādes un dzesēšanas sistēmu attīstība*, VPP-EM-EE-2018/1-0002. Available at https://energy.ec.europa.eu/system/files/2021-10/lv_ca_2020_lv.pdf
16. Cabinet Regulation No. 280. (2019). *Regulations Regarding the Latvian Construction Standard LBN 002-19, Thermotechnics of Building Envelopes.* Available at https://likumi.lv/ta/en/en/id/307966-regulations-regarding-the-latvian-construction-standard-lbn-002-19-thermotechnics-of-building-envelopes
17. Cabinet Regulation No. 222. (2021). *Ēku energoefektivitātes aprēķina metodes un ēku energosertifikācijas noteikumi.* Available at https://likumi.lv/ta/id/322436-eku-energoefektivitates-aprekina-metodes-un-eku-energosertifikacijas-noteikumi
18. Legal Acts of the Republic of Latvia. (2012). *Law on the Energy Performance of Buildings.* Available at https://likumi.lv/ta/en/en/id/253635-law-on-the-energy-performance-of-buildings
19. Construction Information System. (2022). *Ēku energosertifikātu reģistrs.* Available at https://bis.gov.lv/bisp/lv/epc_documents
20. Latvian Open Data Portal. (2022). *Ēku energosertifikātu saraksts*. Available at https://data.gov.lv/dati/eng/dataset/bis_swkx3qxubp9g-wp_zpvciq
21. Gendelis, S. (2021). Ēku energosertifikāta statistika. *Būvinženieris,* 78, 133–138. Available at https://modinst.lu.lv/wp-content/uploads/2021/03/Energosertifikati_BI78.pdf
22. Altum. (2022). Daudzdzīvokļu māju energoefektivitāte 2016–2023. Available at https://www.altum.lv/pakalpojumi/iedzivotajiem/daudzdzivoklu-maju-energoefektivitate-2016-2023/
23. Cabinet Regulation No. 160. (2016). *Darbības programmas "Izaugsme un nodarbinātība" 4.2.1. specifiskā atbalsta mērķa "Veicināt energoefektivitātes paaugstināšanu valsts un dzīvojamās ēkās" 4.2.1.1. specifiskā atbalsta mērķa pasākuma "Veicināt energoefektivitātes paaugstināšanu dzīvojamās ēkās" un 13.1.1. specifiskā atbalsta mērķa "Atveseļošanas pasākumi ekonomikas nozarē" 13.1.1.2. specifiskā atbalsta mērķa pasākuma "Atbalsts daudzdzīvokļu māju siltināšanai" īstenošanas noteikumi*. Available at https://likumi.lv/ta/id/281323-darbibas-programmas-izaugsme-un-nodarbinatiba-4-2-1-specifiska-atbalsta-merka-veicinat-energoefektivitates-paaugstinasanu
24. Official Statistical Portal. (2022). *Average Prices of Energy Resources for Final Consumers.* Available at https://data.stat.gov.lv/pxweb/en/OSP_PUB/START__NOZ__EN__ENC/ENC010/
25. Altum. (2022). *Pieteikšanās ALTUM privātmāju energoefektivitātes uzlabošanas un elektroenerģijas ražošanas programmā sāksies 27. aprīlī*. Available at https://www.altum.lv/pieteiksanas-altum-privatmaju-energoefektivitates-uzlabosanas-un-elektroenergijas-razosanas-programma-saksies-aprili/

sciendo

LATVIAN JOURNAL OF PHYSICS
AND TECHNICAL SCIENCES
2023, N 1

DOI: 10.2478/lpts-2023-0005

OVERVIEW OF MACHINABILITY OF TITANIUM ALLOY (TI6AL4V) AND SELECTION OF MACHINING PARAMETERS

J. P. Gandreddi*[1], A. Kromanis[1], J. Lungevics[1], E. Jost[2]

[1]Riga Technical University,
Department of Mechanical Engineering and Mechatronics,
6b Kipsala Str., Riga, LV-1048, LATVIA
[2]Eplus3D Tech GmbH,
23 Pflugfelder Str., 71636 Ludwigsburg, GERMANY
*e-mail: jyothi-prasad.gandreddi@rtu.lv

Machining of titanium alloy Ti6Al4V is a challenging task for the industry; however, there are some solutions to overcome these difficulties. One of those is optimizing the machining parameters. Machining of Ti6Al4V made by additive manufacturing is an emerging future and is even more difficult when comparing to standard Ti6Al4V alloy. There is lot of invention on Ti6AL4V 3D printed samples, but influence of machining post-printing is lacking. In additive manufacturing of Ti6Al4V alloy, it is necessary to make a finishing operation to improve the surface quality and to ensure precise geometry tolerances. During this process, it may affect the workpiece properties such as microhardness, microstructure, internal defect distribution, internal stresses. During printing there are lots of stresses created, heat treatment is done to normalize the parts. Machining (using milling machine) also causes internal stresses which can damage the surface and part itself. Optimisation of machining parameters and printing parameters can solve this issue. This study gives an overview of selection of machining parameters by considering all the previous relevant research.

Keywords: *Additive manufacturing, adaptive machining, CNC milling, roughness, Ti6Al4V.*

1. INTRODUCTION

The demand for 3D printed titanium alloy parts is increasing widely especially in aerospace industry, medicine because of its high strength and low weight combination [1]. Even though these alloys are expensive, because of their high recyclability rate, the price is negotiable. It is reported that titanium alloys account for approximately 11 % of the fuselage structure weight of the Boeing 777, about 15 % of the Boeing 787 and in the fourth-generation jet fighter F-22 the weight proportion of titanium alloys is about 41 % [2]. In the past, the success of a machining operation was only valued in terms of product quality and cutting tool life, whereas today the most important criterion for success of an operation is its sustainability [3]. By 3D printing, the parts can be printed with precise dimensions, even though many parts require finishing operation to achieve the required surface quality and dimensional tolerances. To achieve the final product, the main problems are printing method and parameters, production time, and machining parameters and adaptability.

Depending on the type of printing method and technique, size of the part, preparing the part itself consumes a lot of time, which can be saved by introducing adaptive machining process for finishing operations. Regarding machining of titanium, much research has already been carried out, but still more attention is to be given to other machining parameters for cost efficient and optimised techniques [1], [4], [5]. During machining the chip gets weld to the tool due to high chemical reactivity of titanium alloy, thus leading to cratering and premature tool failure [6]. To overcome this situation, a proper cutting tool must be selected. The low thermal conductivity of these materials does not allow the heat generated during machining to dissipate from the tool edge. This causes high tool tip temperatures and excessive tool deformation and wear. Since the machining time and cost are high for titanium alloys, the 3D printing could be more focused on cost and time optimisation [7]. High speed machining (HSM) could be one of the preferred options for production times, lower costs, and better-quality products [4]. Adaptive machining is the second option to save the production time and reduce costs. During machining of titanium alloys, the machining parameters such as cutting speed, coolant, feed rate and depth of cut play a significant role because of hard machining nature. In case of machining of 3D printed parts, slow cutting speeds give better surface roughness for the parts made by ABS, and it is reverse for PLA due to high temperatures [8].

Machining of Ti6Al4V alloy made by additive manufacturing higher cutting speeds and feed rates results in poor surface roughness and high cutting forces [9]. For machining of 3D printed titanium alloys, these parameters are even more important because of multiple thin layers in the part. The heat generated during the machining may delaminate the layers and affect the structure of the workpiece. To investigate all these aspects, proper research with a precise analysis is required. In this research paper, an overview of machinability of Ti6Al4V alloy is presented and the selection of machining parameters is explained.

Table 1 shows the composition of Ti6Al4V alloy, consisting of such major components as 90 % titanium, aluminium 5.5 % and vanadium 4.2 %. This alloy belongs to α+β group and is known as grade 5 alloy.

Table 1. Chemical Composition of Ti6Al4V [8]

Chemical Composition	V	Al	Sn	Zr	Mo	C	Si	Cr	Ni	Fe	Cu	Nb	Ti
Weight %	4.2	5.5	0.062	0.003	1.005	0.37	0.022	0.009	<0.001	0.112	<0.02	0.0386	90

2. AN OVERVIEW OF MACHINING OF TITANIUM AND ITS ALLOYS

Titanium is the one of the toughest materials and challenging to perform machining. Despite recent developments and extensive usage of titanium alloys, machining of titanium alloys remains a major industrial concern because of short tool life, low metal removal rates, higher cutting force and temperature, and poor surface quality [5]. There are many parameters to be considered during the machining process. Due to titanium toughness, high cutting pressures are obtained and the cutters receive strong shock, which results in tool wear, damage to workpiece [1], [10]. Previous research suggests many tips to be followed while machining titanium. Titanium is tough and sticky material, so it is necessary to use a very sharp tool to avoid the interruptions. All the cutting speed and feed rates must be selected properly [1]. In general, the machinability of Ti6Al4V is better than Ti555.3 [11] and BTi-6431S [2]. The machinability of titanium alloy can be improved by using a preheating technique called high frequency induction heating [12]. The selection of process parameters is very important in machining [13]. A smooth surface with better MRR can be obtained with optimum combination of parameters [14]. Machining titanium alloys, the main parameters which are to be considered are cutting speed, feed rate, depth of cut, type of coolant, and type of milling tool.

Table 2. Overview of Machining Parameters and its Effects

Material	Operation type	Vc	dc	Feed rate	Tool	Coolant	Description	Ref.
Titanium and its alloys	Turning, Milling, Drilling	150, 300, 450	1.5 mm	0.03, 0.06 mm/tooth	-	Dry, Petroleum based coolant, MQL, Cryogenic cooling, HPC	Cooling methods and its effect	[3]
Ti6AL4V	Turning	45, 90, 180	0.5 mm	0.05, 0.1, 0.2 mm/ rev	Tungsten carbide tool DNGG 150401-SF	-	With increase in Vc, cutting forces increased in SLM Ti6Al4V and decreased in wrought Ti6Al4V, also surface roughness improved. Better surface roughness observed in SLM T-6Al4V.	[9]

Material	Operation type	Vc	dc	Feed rate	Tool	Coolant	Description	Ref.
Ti6AL4V	Milling	80, 127, 200	1.0mm	0.088 mm/tooth	Polycrystalline diamond (PCD) inserts	-	Machining with induction heating – increased tool life. PCD inserts – tool life increased by 169.4 % during preheated machining at 650 ºC.	[12]
Titanium alloys	Turning	31.4 to 157	1.0 mm	0.11 mm/ rev	Coated carbide insert CNMG120404-M5-Tp-3500	Dry	Tool wear mechanism. α alloys – abrasive tool wear. α+β alloys – material adherence on cutting tool. β alloys – deformation of cutting edge	[15]
Ti6AL4V	Turning, LAM, Hybrid	107, 150, 200	0.76 mm	0.075, 0.15 mm/ rev	K68, KC5010	Liquid nitrogen (LN_2)	TiAlN coated carbide tool is 2 to 3 times better than uncoated carbide tool. Increased MRR, tool life and cost savings in hybrid machining process.	[16]
Ti6AL4V	Milling (up)	40– 80	1.0 mm	0.125, 0.15 mm/ tooth	Sandvik^R TPMN 160308-H13A carbide inserts	Dry	For higher tool life and productivity feed rate 0.15 mm/ tooth and Vc = 55m/min should be avoided. Development of AlTiN coated carbide tools.	[17]
Ti6AL4V	Milling	58, 63, 149, 154	-	0.1, 0.5, 1.5, 3.0 µm/tooth	2 and 4 fluted flat end square micro mills	Dry	Feed per tooth is the most influential parameter on surface roughness and burr formation. 2 fluted end micro mill produced better results than 4 fluted micro end mills.	[18]

Material	Operation type	Vc	dc	Feed rate	Tool	Coolant	Description	Ref.
Ti6AL4V	Turning	60*	-	0.08 mm/ rev*	Coated carbide	Lubricant - Blaser Swisslube Vasco 5000, Dry	Effect of lubricant on tool life (increased by 40 %).	[19]
Ti6AL4V	Milling	100, 115	1.0 mm	0.075, 0.1 mm/tooth	Ingersoll CHIP SURFER D12 ball nose cutter	Dry, 30–100 % CO_2, Mineral oil-based emulsion	Advantages of cryogenic milling over dry machining and cooling lubricants.	[20]
Ti6AL4V	End milling	120, 150, 180	0.5, 0.75, 1.0 mm	0.05, 0.075, 0.1 mm/tooth	Kennametal 12A01R020A16ED10, d=12,0mm	-	Taguchi method. Cutting speeds – high effect on temperatures, and less effect on cutting forces. Vc = 150m/min, depth of cut = 0.75mm, feed = 0.075 mm/tooth is suitable for HSM.	[21]
Ti6AL4V	Micro-end milling	31.415	30 µm	0.5, 1.0, 1.5 µm/ tooth	Two-flute tungsten carbide micro-end mill with d = 400µm	Dry	Cutting forces modelling by using ABAQUS / Explicit FEM method	[22]
Ti6AL4V	Turning	45, 60, 75, 90	0.2 mm	0.2 mm/ rev	TPGH080204R-FS	-	Chip formation, tool wear, cutting forces. Machinability of Ti6Al4V is slightly better than BTi6431S	[23]
Ti6AL4V	End milling	30, 40*, 50 60*	2.0*, 2.5*, 3.0, 3.5 mm	0.01*, 0.015, 0.02, 0.025 mm/tooth	Kennametal (HARVI II) Solid carbide end mill d=6.0mm	Optimal amount of coolant	End milling – reduced cutting forces at feed 0.01 mm/tooth, Vc 40 m/min and depth of cut 2.0 mm. Best surface roughness at Vc= 60 m/ min, depth of cut 2.5mm, feed 0.01 mm/tooth.	[24]
Ti6AL4V	Turning	45, 60, 75*	0.25*, 0.5, 0.75 mm	0.25*, 0.3, 0.35 rev/mm	PVD / TiAlN coated carbide inserts	Dry	Surface finish increased with increase in cutting speed. Optimal combination of machining parameters.	[25]

Material	Operation type	Vc	dc	Feed rate	Tool	Coolant	Description	Ref.
Ti6AL4V	Turning	75*	-	0.25mm*	PVD coated carbide	-	Use of Taguchi grey method for optimization. Cutting speed is the most important parameter influencing surface roughness.	[26]
Ti6AL4V	Turning	150*	0.25 mm	0.15mm*	Poly crystalline Diamond (PCD)	MQL	Taguchi method is used to compare the MQL cooling system with dry machining. MQL and PCD inserts are satisfactory tool materials for better surface roughness and hardness.	[27]
Ti6AL4V	Turning	90*, 120	0.8 mm	0.1, 0.2 mm/rev	Uncoated cemented carbide (CCMT 09 T308-KM H13A)	MQL, Dry, MQCL with rapeseed vegetable oil, cooled air, Flooded, Cryogenic	Comparison of lubricants. Proposed using vegetable oil.	[28]
Ti6AL4V	Turning	50, 60, 70*	0.02, 0.035*, 0.05 mm	0.01*, 0.02, 0.03 mm	Multi-layered CVD coated carbide tool	Wet cooling	Surface roughness and roundness.	[29]
Ti6AL4V ELI	Milling	200, 250, 300	1.5 mm	0.03, 0.06 mm/rev	TiAlN + TiN coated and uncoated carbide tools	Dry	Cutting forces decreased with an increase in Vc. Lower cutting forces observed with uncoated tools.	[30]
Ti6AL4V ELI	Turning	120, 170, 220	0.4 mm	0. 2 mm/ rev	Uncoated carbide insert, CNGG 120408-SGF-H13A	Flooded (conventional cooling)	Highest tool wear is observed at cutting speed of 200 m/min and tool life is 2.3 min.	[31]
Ti6AL4V ELI	Turning	120, 170, 220	0.4, 0.5, 0.6 mm	0.1, 0.15, 0.2 mm/ rev	Uncoated carbide insert, CNGG 120408-SGF-H13A	Flooded (conventional cooling)	Investigation on effect of Vc, dc, feed on surface roughness and tool life.	[32]
Ti6AL4V ELI	Turning	200 to 300	1.0 mm	0.2 mm/ rev	-	Dry	Analysis of surface roughness, tool life, and cutting forces.	[33]
Ti6AL4V ELI	Turning	120 to 200	0.4 to 0.6 mm	0.1 to 0.2 mm/rev	Carbide cutting tool	Dry	Analysis of tool wear mechanism	[34]

Material	Operation type	Vc	dc	Feed rate	Tool	Coolant	Description	Ref.
Ti6AL4V ELI	Turning	55, 75, 95	0.1, 0.15, 0.2 mm	0.15, 0.25, 0.35 mm/rev	Uncoated, CVD coated, PVD coated carbide tools	Dry	Microstructure is significantly affected by high cutting speeds (95 m/min)	[35]
Ti6AL4V ELI	Turning	55, 75, 95	0.1, 0.15, 0.2 mm	0.15, 0.25, 0.35 mm/rev	TiAlN coated PVD inserts CCGT 12 04 02 HP	Dry	High surface roughness at high feeds but decreased with an increase in cutting speeds.	[36]
Ti6AL4V ELI	Turning	55, 75, 95	0.1, 0.15, 0.2 mm	0.15, 0.25, 0.35 mm/rev	Uncoated K313 (WC-Co), coated with PVD (KC9225), coated with PVD (KC5010)	Dry	Plastic deformation layer on machined surface was observed at Vc of 90m/min, feed of 0.35mm/rev, and dc of 0.1mm.	[37]
Ti6AL4V ELI	Turning	55, 75, 95	0.1, 0.15, 0.2 mm	0.15, 0.25, 0.35 mm/rev	CVD inserts (KC9225) (CCMT 12 04 04 LF)	Dry	Surface finish mostly affected by nose radius and feed rate. Coated cemented carbide tools produced surface finish is acceptable.	[38]
Ti6AL4V ELI	Turning	55, 75, 95	0.1, 0.15, 0.2 mm	0.15, 0.25, 0.35 mm/rev	CVD inserts with four layers of coating (TiN-Al2O3-TiCN-TiN)	Dry	Analysis of surface quality.	[39]
Ti6AL4V ELI	Turning	55, 75, 95	0.1, 0.15, 0.2 mm	0.15, 0.25, 0.35 mm/rev	PVD – TiAlN coated carbide tool	Dry, flooded	Influence of cutting parameters on machining.	[40]
Ti6AL4V ELI	Turning	120, 170, 220	0.4, 0.5, 0.6 mm	0.15, 0.2, 0.35 mm/rev	-	MQL, Flooded	MQL condition increased tool life by 25 %.	[41]
Ti6AL4V ELI	Turning	50, 65, 80	0.5 mm	0.08, 0.15, 0.2 mm/rev	PVD TiAlN insert. cNMG 120408-QM-1105	Dry	Surface roughness is 0.57 µm and cutting force 54.02 N was obtained at optimum cutting conditions (Vc = 66.97m/min, feed of 0.08 mm/rev).	[42]
Ti6AL4V ELI	Milling	75, 100, 125	0.3, 0.6, 0.9 mm	0.2, 0.25, 0.3 mm/rev	-	Dry	Effect of machining parameters on surface roughness.	[43]

Note: * indicates an optimal parameter. Vc – cutting speed (m/min), dc – depth of cut, MQL – minimum quantity liquid, MQCL – minimum quantity cooling liquid, LAM – laser-assisted machining, HPC – high pressure coolant, SLM – selective laser melting, FEM – finite element method, PVD – physical vapour deposition, CVD – chemical vapour deposition, ELI – extra low interstitials.

The selection of the cutting tool is very important by considering the properties of titanium. The design [44] of tool is very important to machine a hard material like titanium and its alloys. Most used tools are coated carbide tools which help improve the tool life [45]. The factors such as resistance to wear, good heat dissipation properties, ability to resist deformation, type of coating must be considered in the selection of a cutting tool [46]. During machining due to its elastic nature there is a high chance of material sticking to the cutting tool. To avoid such a situation, the tool must be sharper [1]. In case of 3D printed Ti6Al4V, this stickiness presents even more concern because of multiple layers which may result in delamination of layers and internal defects. Due to low Young's modulus, machining of titanium and its alloys has high tool bounce back, it results in stiffness and the tool bounces back from the workpiece. This can be controlled by fixing the tool very tight and tool overhang must be shorter so that it will not pull out due to high cutting forces, pressures, vibrations, and sticky nature of the material itself. [1], [10]. The radial engagement of the tool must be reduced to control heat. For finishing operations, the tool radius in contact must be in small percentage (small engagement) and feed rate must be minimal [1]. The use of coated tools does not show a considerable improvement on the machinability of titanium alloys. The BUE formation in α+β alloy reduces the effectiveness of tool coating [15]. However, a TiAlN [17] coated carbide tool is 2–3 times better than an uncoated carbide tool for hybrid machining [16] and with PVD coated carbide tool, lower temperatures and good surface quality are observed [47]. The cutting temperature and high pressure at the tool-chip interface, built-up edge (BUE) formation [12] [17] and the chemical interaction between the titanium and the tool are the main reasons of the tool wear [3]. An abrasion [13] due to BUE [18] was a major reason of tool wear in α+β alloy [15]. The adhered material is evident slightly more in two flute end mills than 4 flute end mills [18]; thus, an end mill with more flutes is recommended. Tool wear should be low enough to acquire high productivity. A sharp cutting tool with more flutes and small diameter for pockets, long cavities [48] is recommended in machining titanium and the sharpness must be maintained throughout the machining process. The tool radius must not be more than 70 % of that minimum internal radius to ensure plenty of room available for entering the cutting fluid [1]. The tool life can also be increased by using thermally assisted machining [12]. For higher tool life and great productivity, the combination of feed rate 0.15 mm/tooth and cutting speed 55 m/min must be avoided [17]. In Fig. 1, TiCN, Alpha, and TiAlN coated tools have high hardness [49] resulting in high wear resistance [40].

Because of titanium poor heat conductivity, it is hard to take away the heat from the workplace, so a high-pressure coolant can solve this issue [1]. Use of a high-pressure coolant is the best of all as it significantly improves the tool life [3]. By using a coolant in turning Ti6Al4V, the tool life increased by 40 % [19]. Some of the cooling techniques used were dry machining, conventional cooling system, minimum quantity cooling system (MQCL), minimum quantity of lubricant (MQL), cryogenic lubrication [3]. Dry machining is very difficult in taking away the heat resulting in difficulties in production. However, it is useful for sustainability and clean manufacturing. As no coolant is used in dry machining, the impact on environment is minimal. The use of petroleum-based coolants is very expensive, unsustainable due to its impact

on environment and workers' health deterioration. MQL technique resulted in good surface roughness [50], cutting forces, improved tool life and minimal usage of coolant [49]. Cryogenic coolant technique results in better and smooth surface due to residue free coolant evaporation [20]. The usage of liquid nitrogen as coolant results in improved tool life, with 83 % increased MRR and better surface quality [51]. Cryogenic coolant [52] method is very promising; however, a combination of MQL and cryogenic coolant achieves great results [3]. Maximum tool life and auspicious machining condition is obtained by using cooling-vegetable oil on MQL [49].

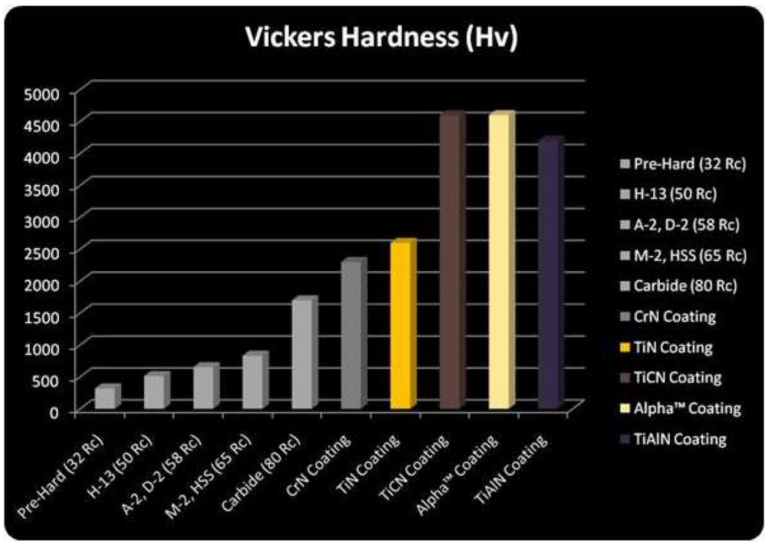

Fig. 1. Different coated tools with Vickers hardness [49].

The most favourable combination for cutting forces is high cutting speeds and low feed rate [13]. The cutting forces generated in machining of Ti6Al4V (α+β) are lower when compared to near α alloys [2]. Mechanical properties such as yield strength and hardness have reasonable influence on cutting forces [9]. The effect of feed rate and depth of cut on cutting forces is higher than the cutting speed effect, whereas cutting speeds have a high effect on temperatures [21], [53]. The cutting forces show a direct relationship with the cutting speed, feed/tooth and stepover, i.e., they increase with an increase in feed/tooth, cutting speed and stepover. The maximum cutting forces were recorded at a high cutting speed with a large stepover [8]. Cutting forces increased with an increase in cutting speed in case of machining of 3D printed Ti6Al4V and opposite in case of wrought Ti6Al4V [9]. From the previous experiments it has been studied that the tool wear is more in case of low-speed machining compared with high speeds. Cutting force is higher in case of a high cutting speed compared to a low cutting speed, which likely results in higher tool wear. An optimum feed of 0.15 mm with 150 m/min with MQL technique is recommended [49]. FEM can be used to simulate the temperatures and cutting forces [22]. In turning operation of Ti6Al4V alloy, the saw-tooth chips are formed at a cutting speed of 90 m/min [23]. At high temperature, work softening appears which makes machining easier but, at the same time, this elevated temperature also accelerates the tool wear and increases surface quality

[13]. Higher cutting speeds result in stable process [54] but have strong effect of tool vibrations on machined surface [18]. By using liquid nitrogen as coolant, the favourable cutting speed is 110 m/min resulting in 91 min tool life [51]. The recommended cutting speed for machining titanium alloys is 60 m/min [10] or less than 60 m/min [16]. For finishing operations, cutting speeds can be 180–240 m/min [10].

In case of machining titanium alloys, feed rate is very crucial as it has a huge effect on surface roughness [50], [55], [56] even with the usage of coolant. If the feed rate increases, the cutting forces increase [13], thus resulting in tool wear. Lower the feed rate, better the tool life, lower cutting forces, and surface roughness. In turning, the feed rate has the strongest influence on tool wear [19]. Low feed rates are recommended in case of high cutting speeds. With an increase in the feed rate, the surface roughness increases due to vibrations and thermal softening of build-up edges [9].

Depth of cut plays a huge role in tool wear and heat generation during machining of titanium alloys. Cutting forces increase with an increase in depth of cut [8]. Cutting forces become more stable at higher depth of cuts (1 mm), however the preferable depth of cut is 0.75 mm [21].

During machining, due to sticky nature of titanium alloys the formation of build-up edge chips [12], [15] is common, which results in faster tool wear and poor surface roughness. These build-up edges can be reduced by increasing cutting speeds, thus contributing to improved surface roughness [9]. Climb milling is one of the best solutions to perform machining on titanium [1]. In down milling, the chips formed are thick at the starting point of cutting and thin at the end point. The burr formation [18] is decreased by 50 % as speed varies from conventional to high speed [57], so that the initial heat will be carried away with chips. Another benefit of this type of milling is that the thin portion of chips does not stick to the tool.

3. CONCLUSION

By considering all these important parameters, it is known that machining standard titanium alloy itself is a challenging task, so one can understand the toughness level of machining titanium alloys made by additive manufacturing. Machining of additive manufactured Ti6Al4V alloys is an emerging challenge to be faced by the industry. Due to hard machining nature and limitations, it is very important to study the effect of machining parameters on surface roughness, distribution of internal stresses, behaviour of microstructure, internal defects, and mechanical properties.

To analyse all these important areas precisely, good equipment with precise readings is required. The internal defects, layer lamination and delamination can be analysed by using computer tomography equipment (CT scan), the surface roughness can be measured by 2D and 3D profilometers from Mitutoyo. In additive manufactured parts it is also important to study the flatness of the sample, which can be done by CMM machine from Mitutoyo. The machining will be conducted on both the wrought Ti6Al4V alloy and 3D printed Ti6Al4V alloy to compare both for giving appropriate results and solutions. Better surface roughness can be achieved with combination of high cutting speeds and low feed rates.

By considering all the previous research and suggestions in Table 2, the effect of machining parameters to be analysed are

cutting speed, depth of cut, feed rate, coolant, cutting tool and type of cutting. Table 3 shows the suggested machining parameters for future research.

Table 3. Selection of Machining Parameters

Cutting tool	D = 6 mm end mill
Coolant	High pressure coolant
Cutting speeds (m/min)	70–240
Feed rate (mm/tooth)	0.01, 0.015, 0.02
Depth of cut (mm)	1.25
Stepover	15 %
Toolpath strategies	One-way, two-way, Helical
Milling type	Climb milling

The planned research will give an overview of effective machining parameters on internal stress and defect distribution in the additive manufactured Ti6Al4V alloy parts (the defect distribution and internal stress distribution is studied by using CT equipment), a solution to improve the mechanical properties and machinability of 3D printed Ti6Al4V alloy. This research is to be continued at Riga Technical University, Latvia.

ACKNOWLEDGEMENTS

1. This research/publication has been supported by the PhD grant of Riga Technical University, Latvia, Europe.
2. The research has been supported by the European Social Fund within the Project No 8.2.2.0/20/I/008 “Strengthening of PhD Students and Academic Personnel of Riga Technical University and BA School of Business and Finance in the Strategic Fields of Specialization” of the Specific Objective 8.2.2 “To Strengthen Academic Staff of Higher Education Institutions in Strategic Specialization Areas” of the Operational Programme “Growth and Employment”.
3. Eplus3D Tech GmbH, Germany sponsored additive manufactured Ti6Al4V alloy samples.

REFERENCES

1. Warfield, B. (2022). *How to Machine Titanium [Tooling, Tips, and Techniques]*. CNCCookbook: Be A Better CNC’er. Available at https://www.cnccookbook.com/how-to-machine-titanium/
2. Gao, Y., Wu, Y., Xiao, J., & Lu, D. (2018). An Experimental Research on the Machinability of a High Temperature Titanium Alloy BTi-6431S in Turning Process. *Manufacturing Review, 5*, 12. https://doi.org/10.1051/mfreview/2018011/
3. Gao, Y., Wu, Y., Xiao, J., & Lu, D. (2022). Improvement of Machinability of Ti and its Alloys Using Cooling-Lubrication Techniques: A Review and Future Prospect. *Journal of Materials Research and Technology, 11*, 719–753.

4. Bandapalli, C., Singh, K., Sutaria, B., & Bhatt, D. (2018). Experimental Investigation of Top Burr Formation in High-Speed Micro-End Milling of Titanium Alloy. *Machining Science and Technology, 22* (6), 989–1011. https://doi.org/10.1080/10910344.2018.1449213
5. Niknam, S. A., Khettabi, R., & Songmene, V. (2014). Machinability and Machining of Titanium Alloys: A Review. *Machining of Titanium Alloys*, 1–30.
6. Kennametal. (2022). *Machining and Manufacturing Made Easy*. Available at https://www.kennametal.com
7. Ahsan, M. M., & Student, M. S. (2016). 3D Printing and Titanium Alloys: A Paper Review. *Eur. Acad. Res, 3* (10), 11144–11154.
8. Polishetty, A., Goldberg, M., Littlefair, G., Puttaraju, M., Patil, P., & Kalra, A. (2014). A Preliminary Assessment of Machinability of Titanium Alloy Ti-6Al-4V During Thin Wall Machining Using Trochoidal Milling. *Procedia Engineering, 97*, 357–364.
9. Polishetty, A., Shunmugavel, M., Goldberg, M., Littlefair, G., & Singh, R. K. (2017). Cutting Force and Surface Finish Analysis of Machining Additive Manufactured Titanium Alloy Ti-6Al-4V. *Procedia Manufacturing, 7*, 284–289.
10. Coromant, S. (2022). *Troublesome Titanium – Tips on Machining this Tough Material*. Available at https://www.sandvik.coromant.com/us/news/technical_articles/pages/troublesome-titanium-tips-on-machining.aspx
11. Arrazola, P. J., Garay, A., Iriarte, L. M., Armendia, M., Marya, S., & Le Maître, F. (2009). Machinability of Titanium Alloys (Ti6Al4V and Ti555. 3). *Journal of Materials Processing Technology, 209* (5), 2223–2230.
12. Ginta, T. L., & Amin, A. N. (2013). Thermally Assisted End Milling of Titanium Alloy Ti-6Al-4V Using Induction Heating. *International Journal of Machining and Machinability of Materials, 14* (2), 194–212.
13. Roy, S., Joshi, K. K., Sahoo, A. K., & Das, R. K. (2018). Machining of Ti-6Al-4V ELI Alloy: A Brief Review. *IOP Conference Series: Materials Science and Engineering 390*, 012112. IOP Publishing.
14. Altaf, M., Dwivedi, S. P., Kanwar, R. S., Siddiqui, I. A., Sagar, P., & Ahmad, S. (2019). Machining Characteristics of Titanium Ti-6Al-4V, Inconel 718 and Tool Steel – A Critical Review. *IOP Conference Series: Materials Science and Engineering, 691* (1), 012052.
15. Joshi, S., Pawar, P., Tewari, A., & Joshi, S. S. (2014). Tool Wear Mechanisms in Machining of Three Titanium Alloys with Increasing β-Phase Fraction. *Proceedings of the Institution of Mechanical Engineers, Part B: Journal of Engineering Manufacture, 228* (9), 1090–1103.
16. Dandekar, C. R., Shin, Y. C., & Barnes, J. (2010). Machinability Improvement of Titanium Alloy (Ti–6Al–4V) via LAM and Hybrid Machining. *International Journal of Machine Tools and Manufacture, 50* (2), 174–182.
17. Jaffery, S., Sheikh, N., Khan, M., & Mativenga, P. (2013). Wear Mechanism Analysis in Milling of Ti-6Al-4V Alloy. *Proceedings of the Institution of Mechanical Engineers, Part B: Journal of Engineering Manufacture, 227* (8), 1148–1156.
18. Rysava, Z., Bruschi, S., Piska, M., & Zidek, J. (2018). Comparing the Performance of Micro-End Mills when Micro-Milling of Additive Manufactured Ti-6Al-4V Titanium Alloy. *MM Science Journal, 2018* (04), 2543–2546.
19. Balažic, M., & Kopač, J. (2010). Machining of Titanium Alloy Ti-6Al-4V for Biomedical Applications. *Strojniski Vestnik/Journal of Mechanical Engineering*, *56* (3).
20. Moritz, J., Seidel, A., Kopper, M., Bretschneider, J., Gumpinger, J., Finaske, T., ... & Ghidini, T. (2020). Hybrid Manufacturing of Titanium Ti-6Al-4V Combining Laser Metal Deposition and Cryogenic Milling. *The International Journal of Advanced Manufacturing Technology, 107* (7), 2995–3009.

21. Krishnaraj, V., Samsudeensadham, S., Sindhumathi, R., & Kuppan, P. (2014). A Study on High-Speed End Milling of Titanium Alloy. *Procedia Engineering, 97*, 251–257.
22. Pratap, T., Patra, K., & Dyakonov, A. A. (2015). Modeling Cutting Force in Micro-Milling of Ti-6Al-4 V Titanium Alloy. *Procedia Engineering, 129*, 134–139.
23. Gao, Y., Wu, Y., Xiao, J., & Lu, D. (2018). An Experimental Research on the Machinability of a High Temperature Titanium Alloy BTi-6431S in Turning Process. *Manufacturing Review, 5*, 12.
24. Vijay, S., & Krishnaraj, V. (2013). Machining Parameters Optimization in End Milling of Ti-6Al-4V. *Procedia Engineering, 64*, 1079–1088. https://doi.org/10.1016/j.proeng.2013.09.186.
25. Satyanarayana, K., & Gopal, A. V. (2013). Optimal Machining Conditions for Turning Ti-6Al-4V Using Response Surface Methodology. *Advances in Manufacturing, 1* (4), 329–339. https://doi.org/10.1007/s40436-013-0047-9
26. Satyanarayana, K., Gopal, A. V., & Babu, P. B. (2013). Analysis for Optimal Decisions on Turning Ti-6Al-4V with Taguchi-Grey Method. *Proceedings of the Institution of Mechanical Engineers, Part C: Journal of Mechanical Engineering Science, 228* (1), 152–157. https://doi.org/10.1177/0954406213480599.
27. Revankar, G. D., Shetty, R., Rao, S. S., & Gaitonde, V. N. (2014). Analysis of Surface Roughness and Hardness in Titanium Alloy Machining with Polycrystalline Diamond Tool under Different Lubricating Modes. *Materials Research, 17* (4), 1010–1022. https://doi.org/10.1590/1516-1439.265114.
28. Deiab, I., Raza, S. W., & Pervaiz, S. (2014). Analysis of Lubrication Strategies for Sustainable Machining During Turning of Titanium ti-6al-4v Alloy. *Procedia CIRP, 17*, 766–771. https://doi.org/10.1016/j.procir.2014.01.112.
29. Vishnu, N., & Aswathy, V. G. (2015). Multi-Response Optimization in Turning of Titanium Alloy Using Grey Relational Analysis. *International Journal of Innovative Research in Science, Engineering and Technology, 4* (12), 11841–11847. https://doi.org/10.15680/IJIRSET.2015.0412025.
30. Sharif, S., Safari, H., Izman, S., & Kurniawan, D. (2014). Effect of High Speed Dry End Milling on Surface Roughness and Cutting Forces of Ti-6Al-4V ELI. Applied Mechanics and Materials, 493, 546–551.
31. Sulaiman, M. A., Haron, C., Ghani, J., & Kasim, M. (2014). Effect of High-Speed Parameters on Uncoated Carbide Tool in Finish Turning Titanium Ti-6Al-4V ELI. Sains Malaysiana, 43 (1), 111–116.
32. Sulaiman, M. A., Che Haron, C. H., Ghani, J. A., & Kasim, M. S. (2013). Optimization of Turning Parameters for Titanium Alloy Ti-6Al-4V ELI Using the Response Surface Method (RSM). *Journal of Advanced Manufacturing Technology, 7* (2), 11–28.
33. Shin, H. G., Yoo, S. H., Park, S. W., & Hong, D. P. (2013). A Study on the Cutting Characteristics and Detection of the Abnormal Tool State in Turning of Ti-6Al-4V ELI. *Applied Mechanics and Materials, 433–435*, 2025–2030. https://doi.org/10.4028/www.scientific.net/amm.433-435.2025.
34. Ghani, J. A., & Haron, C. C. H. (2015). Wear Mechanism of Coated and Uncoated Carbide Cutting Tool in Machining Process. *Journal of Materials Research, 31* (13), 1873–1879.
35. Ibharim, G. A., Arinal, H., Zulhanif, & Haron, C. H. C. (2013). Microstructure Alterations of Ti-6Al-4V ELI During Turning by Using Tungsten Carbide Inserts under Dry Cutting Condition. *International Journal on Engineering and Technology Development, 1* (2), 37–40.
36. Ibrahim, G. A., Che Haron, C. H., & Ghani, J. Abd. (2011). Evaluation of PVD-Inserts Performance and Surface Integrity when Turning Ti-6Al-4V ELI under Dry Machining. *Advanced Materials Research, 264–265*, 1050–1055. https://doi.org/10.4028/www.scientific.net/amr.264-265.1050

37. Ibharim, G. A., Haron, C., & Ghani, J. (2009). The Effect of Dry Machining on Surface Integrity of Titanium Alloy Ti-6Al-4V ELI. *Journal of Applied Sciences, 9* (1), 121–127. DOI:10.3923/jas.2009.121.127.

38. Ibharim, G., Haron, C. H. C., & Ghani, J. A. (2009). Surface Integrity of Ti-6Al-4V ELI when Machined Using Coated Carbide Tools under Dry Cutting Condition. *International Journal of Mechanical and Materials Engineering, 4* (2), 191–196.

39. Gusri, A. I., Haron, C. H. C., Jaharah, A. G., Ahmad, Y. Md. S., Zaid, Y., & Yanuar, B. (2011). Surface Quality of Ti-6%Al-4%V ELI when Machined Using CVD-Carbide Tools at High Cutting Speed. *International conference on Advances in Materials and Processing Technologies, 1315* (1), 1107–1112. DOI:10.1063/1.3552328.

40. Dillibabu, R., Sivasakthivel, K., & Kumar, S. (2013). Optimization of Process Parameters in Dry and Wet Machining of Ti-6AL-4V ELI Using Taguchi Method. *International Journal of Design and Manufacturing Technology, 4* (4), 15–21.

41. Haron, C. H. C., Sulaiman, M. A., Ghani, J. A., Kasim, M. S., & Mohamad, E. (2016). Performance of Carbide Tool in High Speed Turning of Ti-6Al-4V ELI under Conventional Coolant and Minimal Quantity Lubrication. *ARPN Journal of Engineering and Applied Sciences, 11* (7), 4817–4821.

42. Sargade, V.G., Nipanikar, S. R., & Meshram, S.M. (2016). Analysis of Surface Roughness and Cutting Force During Turning of Ti6Al4V ELI in Dry Environment. *International Journal of Industrial Engineering Computations, 7* (2), 257–266. DOI:10.5267/j.ijiec.2015.10.004.

43. Karkalos, N. E., Galanis, N. I., & Markopoulos, A. P. (2016). Surface Roughness Prediction for the Milling of Ti–6Al–4V ELI Alloy with the Use of Statistical and Soft Computing Techniques. *Measurement, 90*, 25–35. https:// doi.org/10.1016/j.measurement.2016.04.039.

44. Bhongale, S., Khandare, Y., & Bobade, S. (2021). Review on Recent Advances in VLSI Multiplier. *IJERT, 10* (11).

45. Kyocera SGS. (2022). *Picking the Right Tools for Machining Titanium*. Available at https://kyocera-sgstool.co.uk/titanium-resources/titanium-machining-and-cutting/picking-the-right-tools-for-machining-titanium/

46. Bryant, W. A. (1998). *U.S. Patent No. 5,718,541*. Washington, DC: U.S. Patent and Trademark Office.

47. Shanker, V. G., Subrahmanya Sai, A. S., Surappa, S., Reddy, C. L. S., & Saketh, R. N. (2021). Machining of Titanium Alloy Grade 5 (Ti-6Al-4V) by Using PVD Coated Cutting Tool Insert. *AIP Conference Proceedings, 2317* (1), 020008.

48. MFG. (2022). *Application of Titanium Alloy Milling in Cutting Tools*. Available at https://www.machinemfg.com/application-of-titanium-alloy-milling-in-cutting-tools/

49. Tanzil, S., & Shaifullah, K. (2022). *A Study on Machinability of Ti-6Al-4V – Process and Optimization*. DOI: 10.13140/RG.2.2.32387.14882/1

50. Ramana, M. V., Vishnu, A. V., Rao, G. K. M., & Rao, D. H. (2012). Experimental Investigations, Optimization of Process Parameters and Mathematical Modeling in Turning of Titanium Alloy under Different Lubricant Conditions. *Journal of Engineering, 2* (1), 86–101.

51. Shokrani, A., & Newman, S. T. (2019). A New Cutting Tool Design for Cryogenic Machining of Ti–6Al–4V Titanium Alloy. *Materials, 12* (3), 477.

52. Pramanik, A., & Littlefair, G. (2015). Machining of Titanium Alloy (Ti-6Al-4V)—Theory to Application. *Machining Science and Technology, 19* (1), 1–49.

53. Krishnaraj, V., Krishna, B. H., & Sheikh-Ahmad, J. Y. (2016). Study of Finish Milling of Titanium Alloy (TI6AL4V). *International Journal of Machining and Machinability of Materials, 18* (5–6), 634–647.

54. Veiga, C., Davim, J. P., & Loureiro, A. J. R. (2013). Review on Machinability of Titanium Alloys: The Process Perspective. *Rev. Adv. Mater. Sci, 34* (2), 148–164.

55. Vijay, S., & Krishnaraj, V. (2013). Machining Parameters Optimization in End Milling of Ti-6Al-4 V. *Procedia Engineering, 64*, 1079–1088.

56. Gandreddi, J. P., Gerins, E., Kromanis, A., & Lungevics, J. (2020). Technological Assurance of Surface Roughness in Pocket Milling. *Annals of DAAAM & Proceedings, 7* (1).
57. Kumar, M., & Bajpai, V. (2020). Experimental Investigation of Top Burr Formation in High-Speed Micro-Milling of Ti6Al4V Alloy. *Proceedings of the Institution of Mechanical Engineers, Part B: Journal of Engineering Manufacture, 234* (4), 730–738.
58. Karolewska, K., & Ligaj, B. (2019). Comparison Analysis of Titanium Alloy Ti6Al4V Produced by Metallurgical and 3D Printing Method. *AIP Conference Proceedings, 2077* (1), 020025. AIP Publishing LLC.
59. NS Tool. (2022). High Efficient Milling on Titanium Alloy Ti-6Al-4V MSXH440R / Power Radius End Mill. Available at https://ns-tool.com/technology/case/sample20/
60. Kozlov, V., & Zhang, J. Y. (2016). Strength of Cutting Tool in Titanium Alloy Machining. *Key Engineering Materials, 685*, 427–431.

sciendo

LATVIAN JOURNAL OF PHYSICS
AND TECHNICAL SCIENCES
2023, N 1

DOI: 10.2478/lpts-2023-0006

METHODOLOGICAL APPROACHES TO THE DESIGN OF A MOBILE TEST FACILITY SIMULATING THE OUTER SPACE

N. Kuleshov[1, 2], S. Kravchenko[1], I. Blumbergs[2],
R. Kubulins[2], V. Shestakov[1, 2]

[1] Cryogenic and Vacuum Systems Ltd.,
7/9 Andreja Str., Ventspils, LV-3601, LATVIA
[2] Institute of Aeronautics, Riga Technical University,
6B Ķīpsalas Str., Riga, LV-1048, LATVIA
*e-mail: valdis.ventspils@gmail.com

The article presents the results of the analysis of methodological approaches to the development of a mobile space simulator test facility following a low-budget project under the conditional name Metamorphosis. The project was performed at the Institute of Aeronautics of Riga Technical University together with Cryogenic and Vacuum Systems Ltd., a company specializing in the development and production of vacuum and cryogenic equipment, with extensive experience in creating technologies used in space research, and development and exploitation of the space environment simulation. The main aim of the study is to find an inexpensive outer space simulator test facility. The study shows that the liquid helium, hydrogen, and neon are significantly more expensive substances than liquid nitrogen, liquid carbon dioxide, liquid ammonia, and organic refrigerants (as well as equipment for their liquefaction). It is desirable to consider a nitrogen system for cooling the workspace due to the physical properties of nitrogen and cheap refrigerants for a projected low-cost simulator test facility. The description of the systems that should be included in the projected mobile space simulator is provided in the article. A generalized scheme of the simulator based on a cryogenic system is also presented.

Keywords: *Cryogenic system, mobile space simulator, vacuum chamber.*

1. INTRODUCTION

Currently, the commercialization of activities in the space industry is rapidly progressing. The direction that ensures the quick and efficient launch of pico- and nanosatellites into low Earth orbits (LEO) is being actively developed [1]. All this has become possible thanks to the enormous achievements of microelectronics, computer science, mass production, and the availability of elements of space systems. The demand comes from commercial organisations, various kinds of societies, educational institutions, etc. [2]. At the same time, each object launched into space and its components must be tested to confirm the safety and declared functional characteristics of space objects and their components following the procedures and standards established by space agencies [3], [4].

Testing is carried out by special testing centres that are currently stationary. The services of these centres are expensive and not always available for small companies, societies, educational institutions, etc. This problem can be solved by creating a mobile ground simulator of space conditions, with the help of which it would be possible to provide testing services at the request of the customer at a place and time acceptable to them [5]. The project called Metamorphosis is being developed at the Institute of Aeronautics of Riga Technical University [6] in cooperation with Cryogenic and Vacuum Systems Ltd. This company specializes in the development and production of vacuum and cryogenic equipment. It has extensive experience in creating technologies used in space research and the development and operation of space environment simulators [7]. Vacuum cryogenic space simulators are whole complexes of devices. The primary element of such a system is a cryogenic system for simulating space conditions. It is a distributed hydraulic system with many pipelines and various units. The cryogenic system includes pumps; refuelling installations that allow charging and discharging refrigerant into storage; sub-coolers that reduce the temperature of cryogenic liquids, i.e., refrigerants; separators, etc.

2. METHODOLOGICAL APPROACHES TO THE DEVELOPMENT OF A MOBILE SIMULATOR OF SPACE CONDITIONS EQUIPPED WITH A PARAMETER CONTROL SYSTEM

The creation of conditions on the ground close to outer space and space flight requirements has been an essential aspect of astronautics since its inception. Their development is constantly being improved along with the development of scientific and technological progress, the expansion of tasks solved by the space industry, etc., and they are becoming more widespread. Simulators of space flight conditions are very diverse in purpose, functions performed, their sizes, etc. [8], [9]. At the same time, customers may have orders for testing at various values of the parameters of the environment, as well as for different objects of research and loads:

- verification of the test objects for the correctness of thermal calculations and heat exchange;
- checking the strength characteristics of the objects;

- studies of the thermal control systems of objects when they are irradiated by the Sun, Moon, Earth;
- other goals.

This requires an extensive set of object tests for various influences arising during their operation in space and during launch: noise, acceleration, aerodynamic loads, and vibration, which can disable them. Special attention is paid to testing to ensure the safety of the tested objects in various emergency situations, etc. Simulators of space conditions save time and money in the development of space objects and their elements, including satellites, since there is no need for real launch of objects in this case.

Until now, there are a limited number of simulators of various types that allow, with a certain degree of accuracy, reproducing individual parameters of outer space for testing objects, their elements, materials, and equipment necessary for the operation of satellites and other objects of a similar purpose in order to determine their suitability for use in outer space, for example, described in [10].

The main properties of the space environment experienced by space objects in the Earth's orbit are deep vacuum, low temperature of outer space, and various types of radiation. The most important of these is a deep vacuum. Therefore, the simulator is based on a vacuum chamber, and moreover, simulators of space conditions are called vacuum chambers [11]. This is the essential part of the installation of the simulator test facility. There are different types of such cameras. The most common option is cylindrical chambers characterised by an optimal mass-to-volume ratio. There may be other options depending on the purpose of the simulator of outer space conditions.

2.1. Vacuum Pumping System

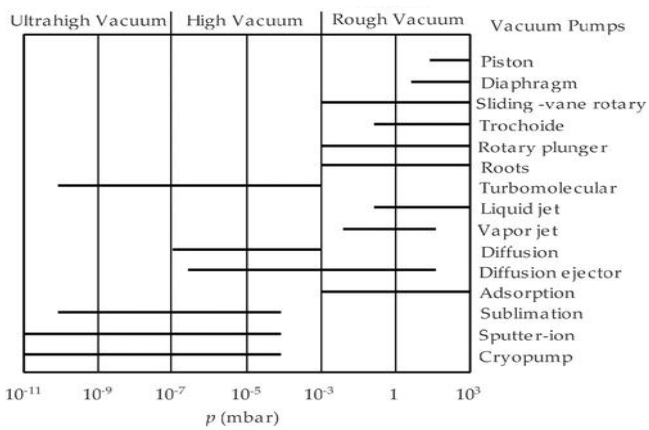

Fig. 1. A vacuum value scale and operating capacities of vacuum pumps [12].

Cryo-condensation and cryo-absorption pumps are used to obtain ultra-high vacuum, high pumping rates, sterile (free from oil and mercury vapor) vacuum. To create a vacuum, air from the chambers is successively evacuated by several stages of vacuum pumps. Two types of devices are usually used for these purposes: one for lowering the pressure inside the vacuum chamber from 1 to 10^{-3} mbar (low vacuum/medium vacuum), and the other for even higher vacuum, pressure from 10^{-3} to 10^{-8} mbar or less (high vacuum). This pumping process consequence is necessary due to the

limitations of the mechanical characteristics of high vacuum pumping units. These can be high-performance mechanical, cryogenic, or turbomolecular pumps. When designing vacuum installations, vacuum pumps are selected so that they meet all test parameters. Figure 1 shows the ranges of operating characteristics of the vacuum pumps used for this purpose in the vacuum scale [12].

The principle of operation of vacuum pumps of the condensation type is that the molecules of a substance having a condensation temperature above the temperature of the cryogenic surface contact it, condenses and are held by the latter. In the molecular flow mode (the mean free path is much greater than the distance between the surfaces), the gas flow Q to the cold surface will be equal to:

$$Q = pA\sqrt{RT \,/\, 2\pi M}, \quad (1)$$

where A is the cold surface area, Q *is* the gas flow, T is the gas temperature, and M is the molecular weight and the theoretical pumping speed per unit of cold surface is determined by the formula:

$$St = Q/pA = \sqrt{RT \,/\, 2\pi M} = 3{,}64\sqrt{T \,/\, M}, \quad (2)$$

where S_t is the theoretical pumping rate l/(s · cm^2). These are the designations adopted in vacuum technology. At T = 293 °K, the maximum pumping rates of nitrogen and hydrogen are 11.8 and 44.2 l/(s · cm^2), respectively. The limiting pressure in chamber p_0 equals the saturated vapor pressure at a cold surface temperature T_x. At pressure $p = p_0$, the pumping speed is zero, i.e., the actual pumping rate S is equal to:

$$S = S_t\,(1 - p_0/p). \quad (3)$$

According to Eq. (2), all molecules in contact with a cold surface are held by it. It means that the accommodation (capture) coefficient ak = 1. Simultaneously with the condensation process, the opposite process occurs, i.e., the evaporation and accommodation coefficient is always less than one ak < 1. It depends on the coefficients of condensation and evaporation; temperatures of gas and cold surface. In addition, the pumping rate and the duration of operation of cryo-condensation pumps depend on the accumulation of a layer of frost on the cold (cryogenic) surface. The thermal conductivity of this layer, as a rule, is low, and the temperature on its surface can significantly exceed the temperature of the cold surface, thus reducing the speed of pumping out of the medium from the vacuum chamber and affecting the level of the achieved vacuum.

2.2. Control of the Vacuum Level

The vacuum chamber allows maintaining a vacuum and simulating the phenomena of thermal and other types of radiation without being influenced by the Earth's atmosphere; these radiations are essential characteristics during the simulation of the outer space thermal environment in the space simulator. High-precision, reliable vacuum sensors are used to control the vacuum level. They are provided with appropriate certificates and allow maintaining the vacuum level during the operation of the vacuum chamber. Parameters of the vacuum level are set from the control panel of the vacuum chamber.

2.3. Temperature Control System (Thermoregulation)

The temperature control system needs to check the impact of the value of the outer space parameters. This impact is characterised by shallow temperatures and variability of the effects of various radiation types (by the sun, Earth, moon, outer space) when the satellite rotates around the Earth. The temperature control system allows maintaining the set temperature following the set of satellite flight modes. The installations of control system elements are characterised by high accuracy of operation. They can consist of various components, including circulation thermostats, thermo-plates, remarkable screens, such as cryogenic ones, etc. All equipment of this type is made of materials capable of withstanding significant temperature fluctuations, shallow temperatures, and high vacuum.

2.4. Automated Control System

This is an essential part of the vacuum chamber of the space simulator because it is responsible for complete control over each stage of the test. The control system necessarily includes devices that allow responding quickly to emergencies. Thus, the space simulator contains a whole complex of systems, for instance: a vacuum system, a thermal system, disinfection systems, a ventilation system, support systems, a solar activity simulator, as well as a control system, and a set of instrumentation. Each of these systems performs a specific task in the testing process, namely:

- The vacuum system creates the desired vacuum levels in a reasonable amount of time and maintains the set vacuum level throughout the test.
- The thermal system most accurately reproduces the radiation of cosmic objects and outer space.
- The function of the disinfection system is to achieve a significant reduction in contamination during testing inside the test facility.
- The ventilation system allows the pressure inside the vacuum chamber to return to an atmospheric pressure value.
- The supply system manages the resources necessary for the regular operation of the installation (water, electricity, compressed air, specific substances, etc.).
- The control system and instrumental complex provide mechanisms and interfaces for controlling various mechanical, electronic, and electromechanical devices that make up the vacuum chamber systems for space simulation.

Figure 2 shows the systems that make up the piping of the vacuum chamber of the outer space simulation test facility.

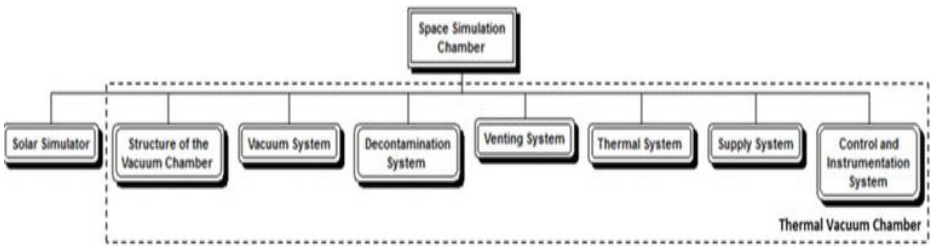

Fig. 2. The systems that make up the piping of the vacuum chamber of the test facility.

Thermal testing is an essential part of space simulator testing to verify the performance and survivability of objects during their operation in outer space. There may be several of them:

- thermal vacuum test (TVT): under this type of test, the object is subjected to a series of high and low-temperature cycles under high vacuum conditions;
- thermal balance test (TBT), the purpose of which is to test the thermal management system of a test facility. Its ability to maintain the temperature of objects within specified limits, etc. [1], [3].

Thermal tests are carried out at different temperature values set at each test level [3]–[5]. Using liquid nitrogen at 77 °K as a cryogenic liquid for the operation of the thermal system, it is possible to reproduce the environment of thermal radiation of the space surrounding the objects with an error of <1 %. As the analysis of the practice of using simulators of space conditions in modelling the space thermal environment shows, there is no need to duplicate the environment of outer space exactly. However, it is necessary to replicate the effects that this environment creates on the materials and components of the objects.

When testing modern leaky orbital objects with a passive thermal control system, the test objects are placed inside a shell capable of absorbing thermal energy because it has a temperature significantly lower, close to absolute zero, than the temperature of the test objects. As a rule, the role of such heat-removing surfaces is played by cryogenic screens – systems of radiation (energy-absorbing) surfaces and associated with them the thermal bridges of heat exchanger pipelines through which the refrigerant circulates. In vacuum chambers for research, development, and testing of materials and equipment, in addition to low pressure, the conditions of illumination and temperature with which the test objects will meet in outer space are also simulated. Based on this condition, there are two types of outer space environment simulators – with the imitation of solar activity that is the part of the vacuum chamber, or the vacuum chamber has not it.

Systems without a solar simulator as part of a vacuum chamber are known as thermal vacuum chambers [13]. These systems also recreate the conditions of the space environment, including solar radiation, using various devices in the test facility. Sunlight is imitated using mercury, xenon, or carbon arc lamps, which are installed outside the vacuum camera. Light and heat from these sources are directed by means of a system of reflectors to the quartz windows of the camera. Then light and heat passing through windows fall on a system of mirrors and lenses already installed inside the camera and are directed and focused on the object under test.

An important task of modeling outer space is to ensure its specific energy dissipation [1]. Therefore, such heat exchange mechanisms as convection heat transfer are not used in these structures. Simulation of processes occurring in space is more reliable if the radiation mechanism of energy transfer is used [15]. Figure 3 shows a variant of the vacuum camera of the space simulator [12].

Based on the above, for the successful development of the Metamorphosis project, it is necessary to determine the basic structure of the simulator, i.e., the cryogenic system, the design of which is an essential part of the entire project.

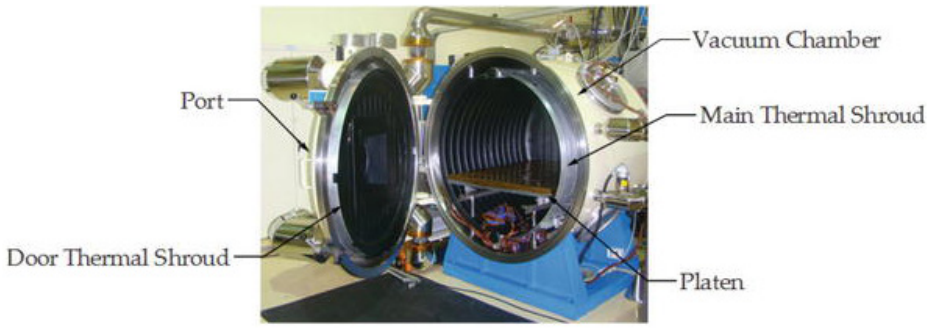

Fig. 3. A variant of the outer space simulator vacuum camera [12].

3. DEVELOPMENT OF A GENERAL SCHEME OF THE CRYOGENIC SYSTEM OF THE SPACE SIMULATOR TEST FACILITY

Based on the terms of the Metamorphosis project on the development of an affordable and accessible mobile simulator of the outer space environment, the type of simulator system was chosen. It was determined that liquid helium, hydrogen, and neon were significantly more expensive substances than liquid nitrogen, liquid carbon dioxide, liquid ammonia, and organic refrigerants (as well as equipment for their liquefaction). Therefore, for the designed low-budget cryogenic system, it is advisable to consider the possibility of using liquid nitrogen, proceeding from the assumption that the temperature range of liquid nitrogen at various pressures is in the range from 63.15 °K at a pressure of 0.123 bar to 126 °K at a pressure of 33.15 bar [1]. The working pressure of the refrigerant is created by a cryogenic pump, at the entrance of which the refrigerant comes from cryogenic storage containing the necessary supply of refrigerant. The selection of pipes through which nitrogen flows, which is produced performed following the factory technical documentation and standards, is also essential. It is planned to place several cryogenic screens in the vacuum chamber of the simulator, through which nitrogen circulates. The energy absorbed by the radiation surface of the cryogenic screen is transferred to the walls of the pipelines by means of heat transfer and from them to nitrogen, which must have sufficient temperature and speed to dissipate the received energy outside the vacuum chamber of the simulator. The refrigerant flow through each cryogenic screen is assumed to be adjustable, making it possible to control the temperature field in the vacuum chamber. The piping structure of the vacuum chamber can be conditionally divided into three blocks:

- The equipment providing refrigerant supply to the cryogenic system of the installation brings the parameters of the medium inside the vacuum chamber to the specified values, passes the refrigerant through the cryogenic system, and, if necessary, removes it from the cryogenic system. This system is connected to external devices such as a refrigerant vapor liquefier, a liquid nitrogen tank (Dewar), a cryogenic pump, etc.
- A vacuum chamber equipped with all the necessary systems for testing the research objects according to the customer's requirements and all structural

elements that provide refrigerant supply to the cryogenic screens with design pressures, flows, and temperatures, and further removal of the refrigerant at their outlet.
- Control and measurement equipment following the research object test plan and equipment for controlling the operation of the simulator as a whole and its separate systems.

Each of the components and assemblies of the cryogenic system must also have sufficient thermal insulation, the necessary safety devices, parameter control elements, and control devices. In recent years, specific polyurethane thermal insulation has been used as an insulating material for these purposes. To guarantee the successful use of thermal insulation, it is necessary to monitor its thermal conductivity in the operating temperature range. Measuring the thermal conductivity of materials is tricky. To solve this problem, Cryogenic and Vacuum Systems Ltd. is developing an installation for measuring the low-temperature thermal conductivity of polyurethane thermal insulation at atmospheric pressure and under vacuum in a helium medium in the temperature range of 10–30 °K, which also significantly contributes to this project as a whole [7].

4. CONCLUSIONS

1. The methodological approaches to the design of a mobile test facility of outer space environment have been developed in Latvia under the Metamorphosis project. Metamorphosis project is an auto trailer with a platform installed on it. The platform carries a test facility that simulates the outer space environment and is equipped with an automated system to stabilize parameters of outer space. The composition of the systems and the structure of the space simulator test facility have been determined. The cryogenic system of the outer space simulator is an essential part that is a distributed hydraulic system with pumps, different pipelines, units, various sensors, etc.
2. To successfully implement the Metamorphosis project, it is necessary to perform thermophysical, hydraulic, strength, and other calculations. The project developers carried out a significant part of these calculations, but the discussion of the obtained results is beyond the scope of this article.

ACKNOWLEDGEMENTS

The research has been financed by the Aeronautics Institute of Riga Technical University, project "Prototype Development of Transportable in Intermodal Traffic Mobile Space Testing Facility "Metamorphosis"" (Metamorphosis, project No. 1.1.1.1/18/A/133).

REFERENCES

1. Kravchenko, S., Panova, N., Kuļešovs, N., Blumbergs, I., & Šestakovs, V. (2020). Analysis of the Technical Implementation Options for Launching a Carrier for Output of Micro Satellites to LEO from an Aircraft Platform (LatLaunch project). In: *61th International Scientific Conference of Riga Technical University* (pp. 16–17), 15–16 October, 2020, Riga, Latvia.
2. Young, D. A., & Olds, J. R. (2021). *Responsive Access Small Cargo Affordable Launch (RASCAL) Independent Performance Evaluation*. Available at https://www.semanticscholar.org/paper/Responsive-Access-Small-Cargo-Affordable-Launch-Yo
3. ASTM International. (2019). *Test Method for Steady-State Heat Flux Measurements and Thermal Transmission Properties by Means of the Guarded-Hot-Plate Apparatus*. ASTM C177-19 standard.
4. European Committee for Standardization (2001). *Thermal Performance of Building Materials and Products - Determination of Thermal Resistance by means of Guarded Hot Plate and Heat Flow Meter Methods - Products of High and Medium Thermal Resistance*. EN 12667:2001 standard.
5. Irimex. (n.d.). *Mobile Test Stand PV 1236*. Available at https://www.irimex.ru/services/catalog/armatura/rubric_501/rubric_510/product_1651/
6. RTU. (n.d.). *Metamorphosis Project.* Available at https://www.rtu.lv/lv/universitate/projekti/atvert?project_number=4127
7. Cryogenic and Vacuum Systems Ld. (n.d.) *Brief Entity Description*. Available at https://www.izm.gov.lv/sites/izm/files/latvian-entries1.pdf
8. *Manned Spacecraft Center in Houston, Texas*. (n.d.). Available at https://ru.wikipediaий.org/wiki
9. Picryl. (n.d.). *NASA Research Center in Ames (Iowa)*. Available at https://picryl.com/ru/media/arc-1944-a-6245-223a9e]
10. ERSTEVAK. (n.d.). *Space Simulators*. Available at https://erstvak.com/catalog/vakuumnaya-sistema-ustanovka/imitator-kosmosa/#1
11. ERSTEVAK. (n.d.). *Vacuum System. Space Simulators.* Available at https://erstvak.com/catalog/vakuumnaya-sistema-ustanovka/imitator-kosmosa/
12. Chisabas, R.S.S., Loureiro, G., & de Oliveira Lino, C. (2018). *Space Thermal and Vacuum Environment Simulation*. Space Flight. DOI: 10.5772/intechopen.73154
13. Vactime. (n.d.). *What is a Thermo-Vacuum Chamber?* Available at https://vactime.net/articles/post/chto-takoe-termovakuumnaya-kamera-ili-kamera-glubokogo-vakuuma-i-kak-ona-rabotaet
14. Butkevich, I. K. (2008). *Cryogenic Systems and Installations*. M.: Publishing Press of BMSTU (in Russian).
15. Kravchenko, S., Panova, N., Kuļešovs, N., & Šestakovs, V. (2020). Methodology of Hydraulic Calculation of Space Simulators' Cryogenic Systems that was Tested within the Project "Cryogenic Insulation Thermal Conductivity Testing System". In: *61th International Scientific Conference of Riga Technical University* (pp. 17–17), 16–17 October, 2020, Riga, Latvia.
16. BLMS. (n.d.). *Space Simulators*. Available at https://blms.ru/space